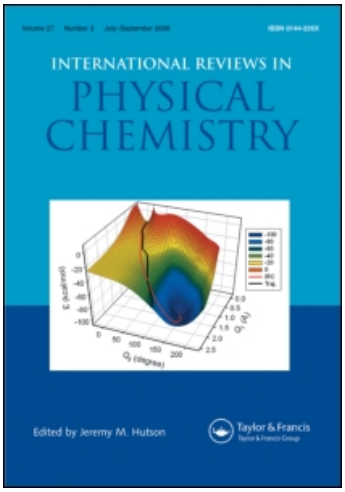

International Reviews in Physical Chemistry
Publication details, including instructions for authors and subscription information:
http://www.informaworld.com/smpp/title~content=t713724383

Laboratory studies of interaction between trace gases and sulphuric acid or sulphate aerosols using flow-tube reactors

Ming-Taun Leu[a]
[a] Earth and Space Sciences Division, Jet Propulsion Laboratory, California Institute of Technology, Pasadena, CA, USA

Online publication date: 26 November 2010

To cite this Article Leu, Ming-Taun(2003) 'Laboratory studies of interaction between trace gases and sulphuric acid or sulphate aerosols using flow-tube reactors', International Reviews in Physical Chemistry, 22: 2, 341 — 376
To link to this Article: DOI: 10.1080/0144235031000087282
URL: http://dx.doi.org/10.1080/0144235031000087282

INT. REVIEWS IN PHYSICAL CHEMISTRY, 2003
VOL. 22, NO. 2, 341–376

Taylor & Francis
Taylor & Francis Group

Laboratory studies of interaction between trace gases and sulphuric acid or sulphate aerosols using flow-tube reactors

MING-TAUN LEU

Earth and Space Sciences Division, Jet Propulsion Laboratory, California Institute of Technology, Pasadena, CA 91109, USA

Stratospheric ozone provides a protective shield for humanity and the global biosphere from harmful ultraviolet solar radiation. In past decades, theoretical models for the calculation of ozone balance frequently used gas-phase reactions alone in their studies. Since the discovery of the Antarctic ozone hole in 1985, however, it has been demonstrated that knowledge of heterogeneous reactions is needed to understand this significant natural event owing to the anthropogenic emission of chlorofluorocarbons. In this review I will briefly discuss the experimental techniques for the research of heterogeneous chemistry carried out in our laboratory. These experimental instruments include flow-tube reactors, an electron-impact ionization mass spectrometer, a chemical ionization mass spectrometer and a scanning mobility particle spectrometer. Numerous measurements of uptake coefficient (or reaction probability) and solubility of trace gases in liquid sulphuric acid have been performed under the ambient conditions in the upper troposphere and lower stratosphere, mainly 190–250 K and 40–80 wt% of H_2SO_4. The trace gases of atmospheric importance include N_2O_5, $ClONO_2$, HCl, HOCl, HNO_3, HONO, HO_2NO_2, $CH_3CO(O_2)NO_2$, CH_3COCH_3, CH_3OH, and C_2H_5OH. In addition, the freezing phenomena of H_2SO_4, the thermodynamics of sulphuric acid monohydrate and the hydrolysis of N_2O_5 on sulphate aerosols will be briefly discussed.

Contents

International Reviews in Physical Chemistry ISSN 0144–235X print/ISSN 1366–591X online © 2003 Taylor & Francis Ltd
http://www.tandf.co.uk/journals
DOI: 10.1080/0144235031000087282

1. Introduction

1.1. *Atmospheric considerations*

The atmosphere consists mainly of a gaseous medium which is composed of N_2, O_2, CO_2 and other trace gas species in that order of decreasing mole fraction. One of the most important trace species in the stratosphere is ozone because it provides a protective shield for humanity and the global ecology from harmful ultraviolet solar radiation. Hence the impact of anthropogenic emissions, such as the release of chlorofluorocarbons (CFCs) [1], aircraft exhaust [2] and others, on the stratospheric ozone layer is of fundamental importance in atmospheric chemistry [3, 4]

The photodissociation of molecular oxygen produces oxygen atoms, which recombine with oxygen molecules to form atmospheric ozone. This process is the primary source of ozone in the stratosphere. Ozone destruction can be catalysed by gas-phase radical reactions, such as

$$\begin{gathered} X + O_3 \rightarrow XO + O_2 (X = Cl, NO, Br, \text{and } OH) \\ \frac{XO + O \rightarrow X + O_2}{\text{net } O_3 + O \rightarrow 2O_2} \end{gathered} \tag{1}$$

and

$$\begin{gathered} Br + O_3 \rightarrow\rightarrow BrO + O_2 \\ Cl + O_3 \rightarrow ClO + O_2 \\ ClO + BrO \rightarrow Br + ClOO \\ \frac{ClOO + M \rightarrow Cl + O_2 + M}{\text{net } 2O_3 \rightarrow 3O_2.} \end{gathered} \tag{2}$$

These fundamental gas-phase reactions have been extensively studied over the last two or three decades. The rate coefficients has been recently compiled in reviews by the NASA Panel on Chemical Kinetics and Photochemical Data for Stratospheric Modeling [5] and the IUPAC Subcommittee on Gas Kinetic Data Evaluation for

Atmospheric Chemistry [6]. It is noted that these data have been widely adopted in stratospheric models dealing with ozone perturbation and others.

Historically, the above-mentioned gas-phase reactions were the major focus of laboratory studies of atmospheric processes until the discovery of Antarctic ozone hole in 1985 [7]. The large increase in ozone depletion and high concentrations of chlorine monoxide (ClO) cannot be explained by these homogeneous gas-phase reactions alone [8]. Several heterogeneous reactions, for example

$$ClONO_2(g) + HCl(a) \rightarrow Cl_2(g) + HNO_3(a), \tag{3}$$

$$HOCl(g) + HCl(a) \rightarrow Cl_2(g) + H_2O(a), \tag{4}$$

$$ClONO_2(g) + H_2O(a) \rightarrow HOCl(g) + HNO_3(a), \tag{5}$$

on the surface of polar stratospheric clouds (PSCs) have been subsequently measured in the laboratory [9–14] and their rate coefficients have been successfully used in the theoretical model for the explanation of the observed high ClO concentrations [5, 6]. This suggestion has been proved beyond any reasonable doubt to be responsible for the huge loss of atmospheric ozone through the powerful catalytic ClO–ClO reaction chain [15] and other catalytic reaction mechanisms (1) and (2) in the springtime of the Antarctic stratosphere.

PSCs are thought to consist of two types:

- Type I PSCs are formed at ambient temperatures between 185 and 200 K and consist of submicron- or micron-sized aerosols containing either (a) solid crystals of nitric acid trihydrate or (b) ternary solutions of HNO_3–H_2SO_4–H_2O mixture [16–20].
- Type II PSCs are observed at colder temperatures, below 185 K, and consist of larger water ice crystals 10–100 μm in diameter [16–18].

The abundance of type I PSCs is much higher than that of type II in the polar stratosphere [18].

In the mid-latitude stratosphere, sulphate aerosols contain H_2SO_4 with composition in the range from 60 to 80 wt%. At warmer temperatures and higher acidic concentrations, reactions (3) and (4) are somewhat less important because the solubility of HCl into liquid H_2SO_4 is quite small. However, reactions (3) and (4) play an important role in cold winters at higher latitudes because H_2SO_4 solutions become more dilute, the solubility of HCl is significantly enhanced and these reactions are very rapid. In addition, the hydrolysis of N_2O_5 in liquid H_2SO_4

$$N_2O_5(g) + H_2O(a) \rightarrow 2HNO_3(g) \tag{6}$$

has also been thought to be important because of a very large reaction probability (~ 0.1) at stratospheric temperatures [3, 4]. Reaction (6) plays a key role in maintaining the ratio of NO_xNO_y and in activating chlorine species in the stratosphere because the conversion of active nitrogen (NO_x) to nitrogen reservoir (NO_y) is rapid. It is noted that NO_xNO_y is defined as the ratio of primary oxides of nitrogen, NO and NO_2, to their oxidation products, such as HNO_3, HO_2NO_2 (peroxynitric acid, PNA) and $CH_3CO(O_2)NO_2$ (peroxyacetyl nitrate, PAN).

In the later 1980s and early 1990s reactions (3)–(6) on type I(a) and type II PSCs were previously investigated in our laboratory and the results have been documented [12, 13, 21–24]. However, in recent years we have focused our studies on H_2SO_4

aerosols and type I(b) PSCs [25, 26]. Moreover, we have also undertaken a series of studies on the interaction between liquid sulphuric acid and nitrous acid (HONO) [27], PNA [28], PAN [29], acetone [30], methanol [31] and ethanol [32]. Furthermore, we have also investigated ammonium-containing sulphate aerosols which are also important in the global troposphere [33]. These results will be summarized in section 3.

1.2. *Gas–aerosol interactions*

Gas aerosol interactions involve a number of transport and chemical conversion processes as shown in figure 1 [34, 35]. The processes include gas diffusion, mass accommodation and evapouration to and from the interface, and diffusion, solubility and reaction in the condensed phase. In some cases, interfacial diffusion and reaction may also play a role in the net uptake when the liquid-phase diffusion and solubility are very slow.

The term 'uptake coefficient' is commonly used in theoretical models relevant to atmospheric processes. In general, the uptake coefficient can be classified into two types of process. If the uptake is physical and reversible, the rate of this process is also called as the sticking coefficient. Since the process is reversible, the rate is important in the partition of concentrations between the gas phase and condensed phase on the basis of the physical Henry's law solubility constant, H. If the uptake is reactive and irreversible, however, the rate coefficient can be described as reaction probability, γ, where

$$\gamma = \frac{\text{number of gas molecules removed by reactions in the condensed phase}}{\text{number of gas molecules colliding with the condensed phase}}. \quad (7)$$

By definition, γ can have values between 0 and 1. The concentration of aerosols in the lower stratosphere and upper troposphere is quite low for a reaction to play an important role in atmospheric chemistry, γ values need to be high ($> 10^{-3}$). In some cases (e.g. methanol and ethanol) the uptake may comprise these two processes; we will use the uptake coefficient.

The uptake coefficient can be approximated as

$$\frac{1}{\gamma} = \frac{1}{\alpha} + \frac{1}{\gamma_{\text{sol}} + \gamma_{\text{rxn}}} \quad (8)$$

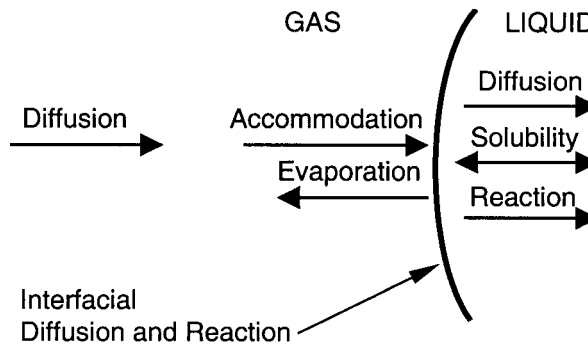

Figure 1. Schematic diagram of physical and chemical processes that determine the net uptake of trace gas species by aerosols.

where α is the mass accommodation coefficient, defined as the ratio of the number of gas molecules absorbed by the condensed phase to the number of gas molecule collisions with the condensed phase. The term α can have values between 0 and 1. However, α is typically near unity for the laboratory studies of heterogeneous chemistry in liquid H_2SO_4 at stratospheric temperatures. Hence, we can neglect the $1/\alpha$ term in the resistance model if $1/\alpha \ll 1/(\gamma_{rxn} + \gamma_{sol})$ [9]. The uptake coefficient, γ, can be approximately equal to the sum of γ_{rxn} and γ_{sol}:

$$\gamma_{rxn} = \frac{4HRT}{\omega}(D_l k_l)^{1/2} \tag{9}$$

$$\gamma_{sol} = \frac{4HRT}{\omega}\left(\frac{D_l}{\pi t}\right)^{1/2}. \tag{10}$$

In these equations t is the time the trace gas is exposed to the liquid H_2SO_4, R is the gas constant, D_l is the liquid-phase diffusion coefficient and ω is the mean molecular velocity of the trace gas. If reaction is predominantly important, equation (9) can be used to determine the liquid-phase reaction rate (k_l) from the observed γ values. However, if solubility dominates, equation (10) can be used to derive the Henry's law constant from the plot of $1/\gamma(t)$ versus $t^{1/2}$. In the kinetics studies using cylindrical flow-tube reactors as discussed in the next section, we make corrections for the observed first-order rate, k, due to the effects of radial and axial diffusions in the reactor according to the theoretical treatment by Brown [36]. We then obtain the γ values from k. Details will be given in section 2.

As discussed above, the liquid-phase diffusion is one of the important processes shown in figure 1. Two methods were used to estimate the liquid-phase diffusion coefficient. The first method was suggested by Klassen *et al.* [37]. The diffusion coefficient in liquid is given by

$$D_l = \frac{cT}{\eta} \tag{11}$$

where T is the temperature, η is the viscosity of liquid and c is a constant determined from the molar volume of solute (Le Bas additivity rules). Wilke and Chang [38] empirically determined the value of c for the species in liquid sulphuric acid,

$$c = \frac{7.4 \times 10^{-8}(\kappa_{solvent})^{1/2}}{V_A^{0.6}} \tag{12}$$

where $\kappa_{solvent}$ is a solvent-dependent empirical factor (e.g. $\kappa_{solvent} = 64$ for H_2SO_4) and V_A is the Le Bas molar volume of solute A at its normal boiling temperature (e.g. $V_A = 74\,cm^3\,mol^{-1}$ for acetone) [39]. For example, the value of c was found to be 4.47×10^{-8} for acetone in H_2SO_4 [30]. In general, D_l decreases with decreasing temperature and increasing acid concentration.

We also calculated the diffusion coefficient (e.g. for acetone) in H_2SO_4 by the cubic cell model [40]:

$$D_l = \frac{RT\rho\lambda^2}{6\eta M_{solute}} \tag{13}$$

and

$$\lambda = \frac{1}{2}\left\{ d + \left[\frac{x M_{SO_4^{2-}} + (1-x) M_{H_2O}}{\rho} \right]^{1/3} \right\} \tag{14}$$

where ρ is the density of liquid H_2SO_4 and x is the H_2SO_4 mole fraction. M_{solute}, $M_{SO_4^{2-}}$ and M_{H_2O} are the molecular weights of solute, SO_4^{2-} and H_2O respectively. For example, the effective molecular dimension (d) was taken to be 0.55 nm for acetone. [41, 42]. The cubic cell method generally finds larger values of D_l than the Le Bas viscosity method by 20–50%. The method suggested by Klassen *et al.* [37] is probably more accurate than the cubic cell method because the cubic cell model assumes the shape of molecules. It should be noted that protonation, ionic reaction and other reactions occur rapidly in liquid H_2SO_4 solution and that H* (the effective Henry's law constant) instead of H (the physical Henry's law constant) was actually measured in our laboratory studies of solubility in H_2SO_4 [28–30].

1.3. *Thermodynamics of the H_2SO_4–H_2O binary system*

Figure 2 shows a plot of the data of the freezing point versus acid composition of hydrated H_2SO_4 [42, 43]. The data (open triangles) are the observed freezing temperatures of various H_2SO_4 solutions in the flow-tube–mass spectrometer apparatus. The horizontal bar denotes the composition range over which the films were held below 190 K without freezing. The smooth broken curves represent equilibrium acid compositions of sulphate aerosols at H_2O mixing ratios of 5.0, 3.0 and 1.5 ppmv at 16 km.

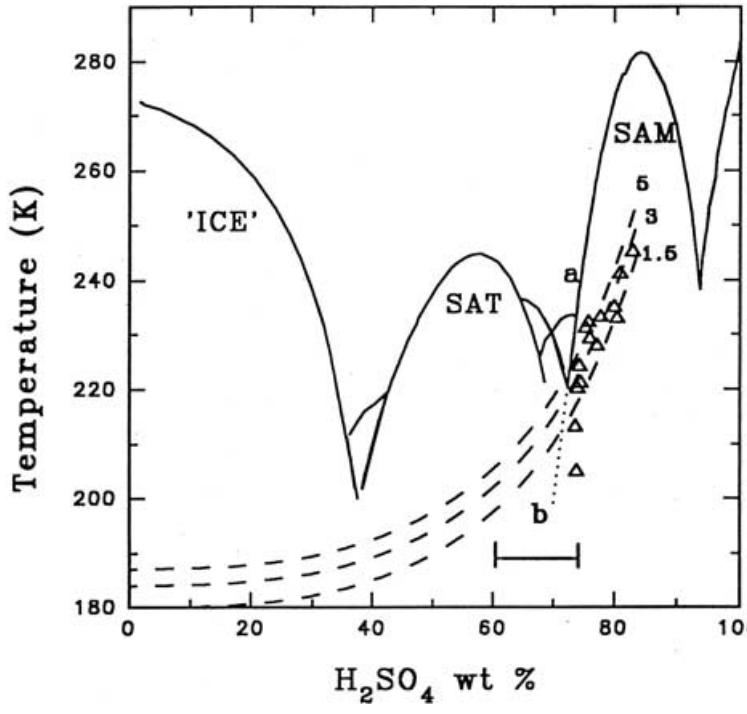

Figure 2. Liquid–solid phase diagram for the H_2SO_4–H_2O system (SAM, sulphuric acid monohydrate; SAT, sulphuric acid tetrahydrate). Open triangles indicate the freezing temperatures in various H_2SO_4 compositions. Adopted from Zhang *et al.* [43].

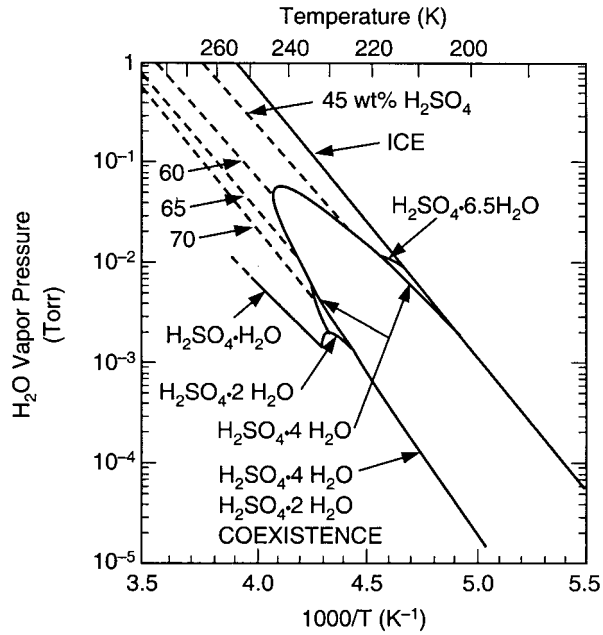

Figure 3. Water vapour pressures as a function of temperature for the H_2SO_4–H_2O system. Acid compositions are determined from the water vapour pressures and temperatures in the reactor.

Figure 3 shows a plot of the water vapour pressure versus inverse temperature [9]. The broken lines represent vapour pressures of liquids at constant acid compositions from 45 to 70 wt%. Acid compositions in our studies are routinely calculated from the water vapour pressures and temperatures. Both SAM [43] and SAT [44] are also readily formed on the wall of the reactor.

Two of the most important characteristics of H_2SO_4 as a reaction medium have long been recognized: its protonating ability and its affinity for water (or dehydrating power). For example, the protonation of a substance such as chlorine nitrate ($ClONO_2$),

$$ClONO_2 + H_2SO_4 \rightleftharpoons ClONO_2H^+ + HSO_4^-, \tag{15}$$

has been thought to be the primary step in reactions (3) and (5) in the condensed phase [45]. Similarly, protonation also occurs in reactions involving N_2O_5, HONO and organics [35]. Dehydration by concentrated H_2SO_4 has also been thought to occur in the interaction with methanol [32, 46]:

$$CH_3OH + H_2SO_4 \rightleftharpoons CH_3HSO_4 + H_2O. \tag{16}$$

We will discuss these subjects later in section 3.

2. Experimental methods

In this section we will briefly discuss the experimental methods used in the investigation of atmospheric heterogeneous chemistry. The subsections discuss the flow reactor, mass spectrometry and aerosol analysis. A theoretical approach using these measurements in the determination of uptake coefficient or reaction probability

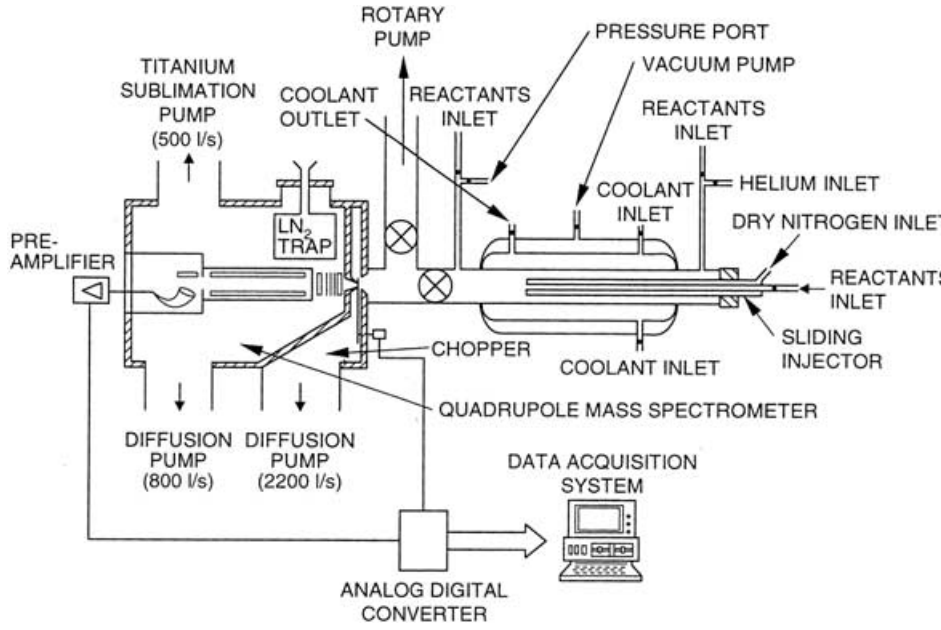

Figure 4. Schematic diagram of the flow-tube reactor coupled to an electron-impact ionization mass spectrometer.

is discussed. Detailed descriptions have been given in previous publications [23, 33, 47].

2.1. *Flow reactor*

The cylindrical flow reactor was made of borosilicate glass, typically 60 cm in length and 2.5 cm inside diameter (see figure 4). Temperature was regulated by circulating cold methanol through the outside jacket surrounding the flow reactor and measured by a thermocouple attached to the middle section. The pressure inside the reactor was monitored by a high-precision capacitance manometer which was located a few centimetres from the reactor at the downstream end. The measured pressure was corrected for the viscous pressure gradient between the measurement point and the midpoint of the reactor. The carrier gas was helium in the wall-coated reactor and nitrogen in the aerosol reactor. The reactants, such as $ClONO_2$, were added through a sliding borosilicate injector as shown in figure 4. Typically, average flow velocities in the range 300–3000 cm s^{-1} and total pressures of 0.3–1.0 Torr were used in the wall-coated reactor. However, flow velocities of 5–10 cm s^{-1} and a total pressure of $\sim$730 Torr were held in the aerosol reactor. A large valve located at the downstream end of the neutral reactor was used to regulate the flow velocity and the total pressure.

2.2. *Data analysis*

The uptake coefficients (or reaction probabilities) were determined as follows. The loss rates of reactants, k, were measured as a function of injector position, z, according to the following equation:

$$k = -v\frac{\mathrm{d}\ln(C)}{\mathrm{d}z} \tag{17}$$

where C is the reactant concentration and v is the average flow velocity. The reaction time was calculated by using $t = z/v$. In each experiment we calculated the cross-sectional area of the reactor and then the flow velocity. The first-order rate constant, k, was calculated from the slope of a linear least-squares fit to the experimental data. The axial and radial gas-phase diffusion corrections for k were made for a cylindrical flow-tube using the data analysis procedures reported by Brown [36]. The corrected rate for gas-phase diffusion was designated by k_g. The above-mentioned treatment was applied to the laboratory studies using both the wall-coated reactor and the aerosol reactor.

In the cylindrical wall-coated reactor, reactions occur on the inner surface of the reactor. The uptake coefficient was calculated from the k_g value from

$$\gamma = \frac{2rk_g}{\omega + rk_g} \tag{18}$$

where r is the radius of the flow rector and ω is the mean molecular velocity of the reactant. γ values in the range from 1×10^{-4} to ~ 0.3 can be determined.

The uptake coefficient was also determined from k_g using the aerosol reactor after subtracting the contribution from surface reactions on the inner surface of the reactor. Using the data of size distribution, we determine the uptake coefficient

$$\gamma = \frac{4k_g}{A\omega} \tag{19}$$

where A is the surface area density of aerosols measured by the scanning mobility particle spectrometer (SMPS, TSI model 3934; see section 2.4 for a detailed description) and ω the mean molecular velocity of reactant. However, all of the data shown in section 3 were analysed by a more accurate method developed directly from the size distribution data [33, 48]:

$$k_g = \sum_i k(r_i) = \sum_i \frac{\gamma N_i \omega \pi r_i^2}{1 + \gamma(0.75 + 0.283Kn_i)/Kn_i(Kn_i + 1)}. \tag{20}$$

The Knudsen numbers

$$Kn_i = 3D_g/\omega r_i \tag{21}$$

were calculated for various particle radii (r_i) of aerosols. This method takes the Kelvin effect for smaller aerosols into account. Typically, the difference in γ values determined by equations (19) and (20) is less than 10–20% for the results of N_2O_5 uptake by sulphate aerosols. We have assumed that the shape of the aerosol particle is spherical in the data treatment. In general, γ values in the range from 1×10^{-3} to ~ 1.0 can be determined by this method.

2.3. *Mass spectrometry for trace gas analysis*

Two types of quadrupole mass spectrometers utilizing electron-impact ionization or chemical ionization were used for these laboratory investigations. These instruments are discussed in the following sections.

2.3.1. *Electron-impact ionization mass spectrometer*

We have constructed a differentially pumped quadrupole mass spectrometer (QMS) using an electron-impact ionization method. High-sensitivity detection was achieved by properly designing the sampling pinhole in the first vacuum chamber and by using ultrahigh vacuum techniques with either pulse-counting or analogue electronics. The front vacuum chamber was evacuated by a $2500\,l\,s^{-1}$ diffusion pump (Varian, model VHS-6). The vacuum chamber in which the mass spectrometer was installed was evacuated by another diffusion pump of $1200\,l\,s^{-1}$ capacity (Varian, model VHS-4). These diffusion pumps were provided with liquid-nitrogen cold traps in order to prevent backstreaming of oil vapour. Two high-capacity rotary pumps were also used in conjunction with the diffusion pumps to evacuate the vacuum chamber. A titanium sublimation pump ($\sim 500\,l\,s^{-1}$) surrounded by a liquid-nitrogen-cooled baffle was also available for further evacuation in the chamber housing quadrupole rods. The ultimate vacuum was better than 10^{-10} Torr after the vacuum chamber was baked at 500 K for 2 or 3 days.

The QMS, supplied by Extrel Corporation, consisted of a cross-beam electron-impact ionizer, a set of quadrupole rods (22.9 cm long by 1.6 cm diameter), a high-gain electron multiplier and a C-50 electronics module. The mass spectrometer can be operated from 1 to 250 amu. In the early experiments a pulse-counting technique was used for detection because of low signal intensity. The channeltron output of the QMS was sent to an amplifier–discriminator and the transistor–transistor logic (TTL) pulse output from the discriminator was registered in a counter in synchronization with the beam stopper that was located in the first vacuum chamber. Typically, the S/N ratio was about unity at an HCl partial pressure of 5×10^{-8} Torr. Similar detection sensitivities for the other reactants were also determined.

In later experiments we switched to the analogue mode instead of counting mode for running this mass spectrometer. However, there is no significant difference in detection sensitivities between these two methods.

2.3.2. *Chemical ionization mass spectrometer*

A schematic diagram of the chemical ionization mass spectrometer (CIMS) apparatus is shown in figure 5. The ion flow reactor was constructed from a stainless steel tube 127 cm in length and 7.0 cm inside diameter. A large flow of helium or nitrogen, 3–10 standard $l\,min^{-1}$ at 293 K, was passed through the reactor at a constant pressure in the range 0.2–0.5 Torr. A large capacity booster pump (Edwards High Vacuum, model EH2600, $6101\,s^{-1}$) was used to evacuate the ion flow reactor. The average flow velocity used in the ion flow reactor was typically about 100–$160\,m\,s^{-1}$ in these experiments. A small flow of SF_6, 1–5 standard $cm^3\,min^{-1}$ at 293 K, was mixed with the helium carrier and SF_6^- ions were formed by electron attachment. The electrons were produced by passing a current (6–10 A) through a filament located at a side-arm port of the reactor. The filament material was tungsten, rhenium or thoriated iridium. SF_6^- ions were allowed to react with the trace gas species from the wall-coated reactor or aerosol reactor; for example, HNO_3 by the reaction

$$SF_6^- + HNO_3 \rightarrow NO_3^-(HF) + SF_5 \quad (k = 1.8 \times 10^{-9} cm^3\,s^{-1}\,[49, 50]). \qquad (11)$$

These ions were then effused through a molybdenum orifice (0.5 mm in diameter) and collimated by a set of ion lenses. The first lens was separated from the

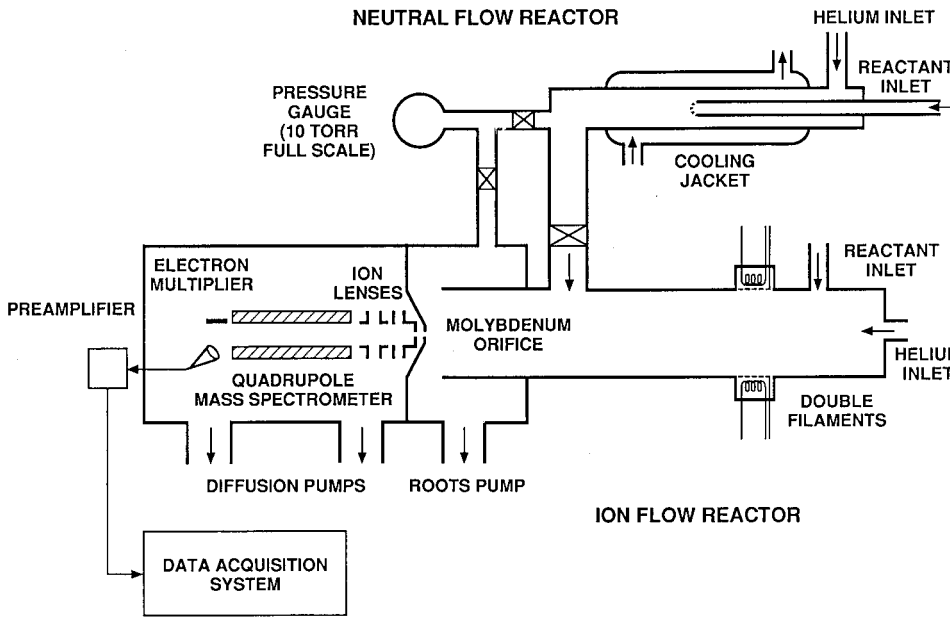

Figure 5. Schematic diagram of a CIMS. Either a wall-coated reactor or an aerosol reactor can be interfaced to this apparatus.

molybdenum orifice about 0.5 cm and was biased by a small voltage ($\sim$1–10 V) in order to focus the ions through the lens system.

A QMS (a set of quadrupole rods 22.9 cm in length and 1.6 cm in diameter powered by a C-60 electronics module) was used to analyse these ions (for example, 146 amu for SF_6^- and 82 amu for $NO_3^-(HF)$). The ions were amplified by a conversion dynode–electron multiplier and then recorded by an electrometer (Extrel Corp., model 031-2). A personal computer was used to acquire the data for further analysis. Preparing a known amount of HNO_3 vapour in a helium carrier in a glass vessel and measuring its flow rate accomplished the calibration procedure. The dynamic range is linear up to 3×10^{11} molecules cm^{-3}. The detection sensitivity for HNO_3 molecules using this technique is about 2×10^8 molecules cm^{-3} (or 6×10^{-9} Torr and $S/N = 1$ for 1 s integration). Similar detection sensitivities for other molecules, for example N_2O_5, were also determined [47].

2.4. *Aerosol analysis*

Figure 6 shows the components of the experimental set-up used to control aerosol formation and measurement. Ammonium sulphate ($(NH_4)_2SO_4$) and ammonium bisulphate (NH_4HSO_4) aerosols were formed by using a constant output atomizer (TSI, model 3075) filled with 0.1% by mass solutions in distilled water. This dilution provided sufficient aerosol output for uptake measurements without blocking such aerosol measurement instruments as the regulating valves and inlet impactor.

Aerosols were produced by the expansion of compressed, dry N_2 through an orifice, from which the liquid to be atomized was drawn from the reservoir. The N_2 carrier passed through a molecular sieve trap in order to remove the impurities.

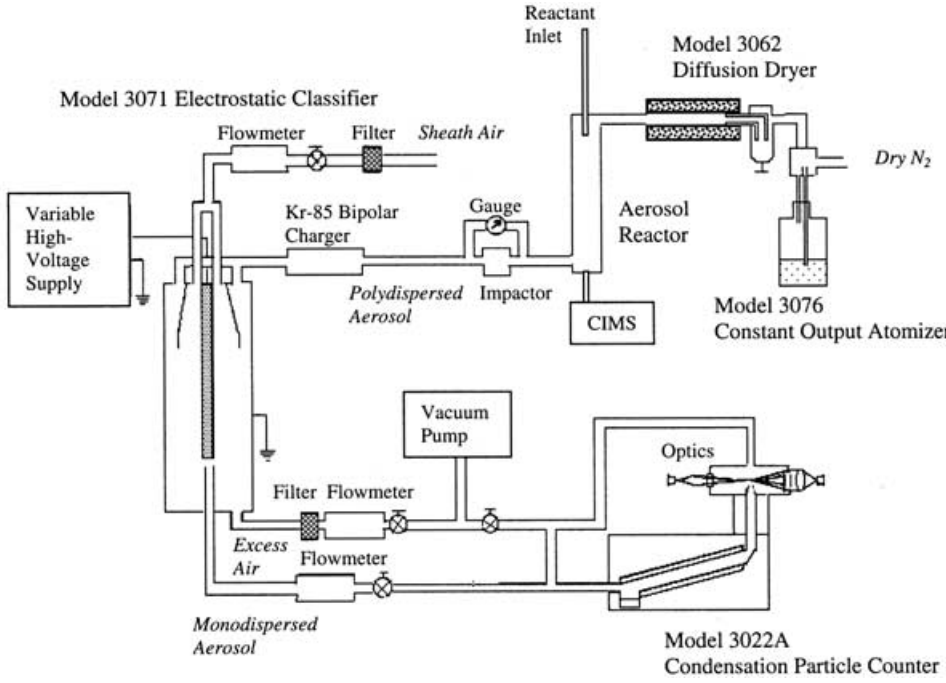

Figure 6. Detailed diagram of the aerosol instruments used in the aerosol generation and in the determination of aerosol size distributions.

Large droplets impacted upon the wall of the atomizer and returned to the reservoir, while a fine spray of particles left the generator. This flow then passed through a diffusion dryer (TSI, model 3062), which was used to control partially the relative humidity of the final aerosol flow and to allow large aerosol particles to settle to the wall, providing a more stable particle size distribution. Further change of the aerosol humidity was achieved by adding water vapour or dry N_2 flows to the aerosol stream. Relative humidity was measured at the bottom of the flow reactor with a fast-response, digital hygrometer (VWR, model 35519-041), which was protected from irreversible aerosol coating on the sensor surface by a tube filter (Balston, DFU-9930-05 DF) inserted into the exit tube of the flow reactor. It is noted that the relative humidity measurements were performed in the absence of N_2O_5 in order to prevent the contamination of the sensor element.

Sulphuric acid aerosols were produced by a different method to that described above and based solely on SO_3 hydrolysis. The first step in aerosol production was mixing SO_3 vapour and moisturized N_2 streams into a glass reactor, allowing reaction and nucleation. SO_3 was supplied from fuming H_2SO_4 in an N_2 carrier. This aerosol stream then passed into a condensation chamber containing sulphuric acid of known composition. The residence time in this chamber was long enough to allow aerosol particles to reach equilibrium in the exchange of water vapour above the solution. Because the times required to reach equilibrium vary greatly as a function of temperature and composition, the range of aerosols that could be produced by this source was limited.

The characterization of aerosols was carried out by the scanning mobility particle spectrometer (SMPS), which includes an electrostatic classifier, a condensation

particle counter, a personal computer and operational software. Following passage through the flow reactor, the aerosol flow was channelled into an electrostatic classifier (TSI, model 3071A). After exposure to an ^{85}Kr bipolar charger, aerosol particles were selected according to their electrical mobility before being passed to a condensation particle counter (TSI, model 3022A). By scanning the classifier voltage, we obtain the particle size distribution. Since particle separation depends on electrical mobility and not particle size, a correction to the particle distribution must be made to account for multiply charged aerosols. On the basis of this information, a variety of aerosol properties including total particle density, surface area and aerosol volume can be calculated. In particular, we need to determine the surface-to-volume ratio of the aerosol flow for the kinetic studies. It should be noted that the calculation using the SMPS software is based on the assumption that the aerosol particles are spherical.

3. Results and discussion

3.1. *Sulphuric acid*

In the past few years we have extensively investigated the solubility and reaction of trace gases in liquid H_2SO_4 films and sulphate aerosols. These gases include $ClONO_2$, N_2O_5, hypochlorous acid (HOCl), HCl, HONO, PNA, PAN, acetone, methanol and ethanol. In the following sections we will briefly discuss these results. Details were given in previous publications [25–32].

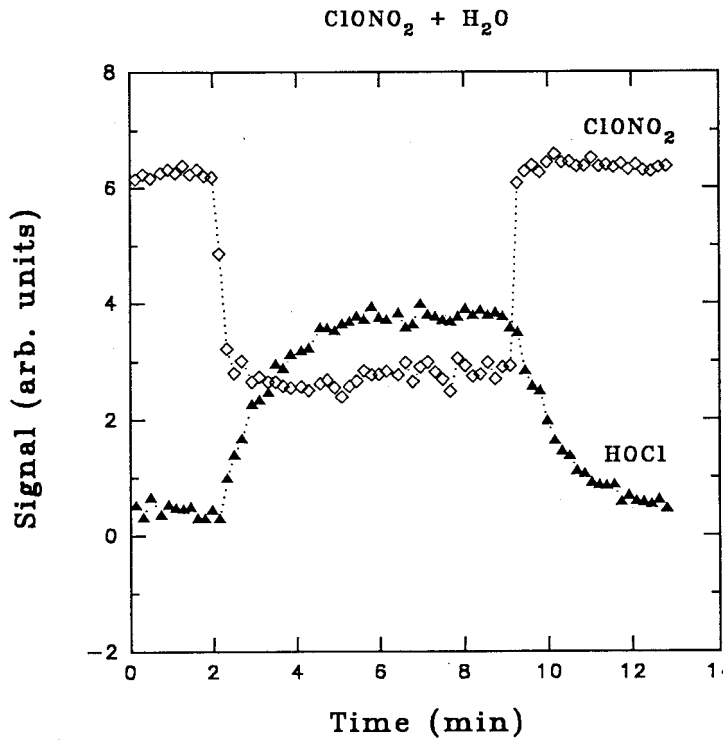

Figure 7. Temporal profiles of $ClONO_2$ (open diamonds) and HOCl (full triangles) as $ClONO_2$ was exposed (at $t \sim 2$ min) and unexposed (at $t \sim 9$ min) to a 10 cm length of liquid H_2SO_4 film coated on the reactor wall.

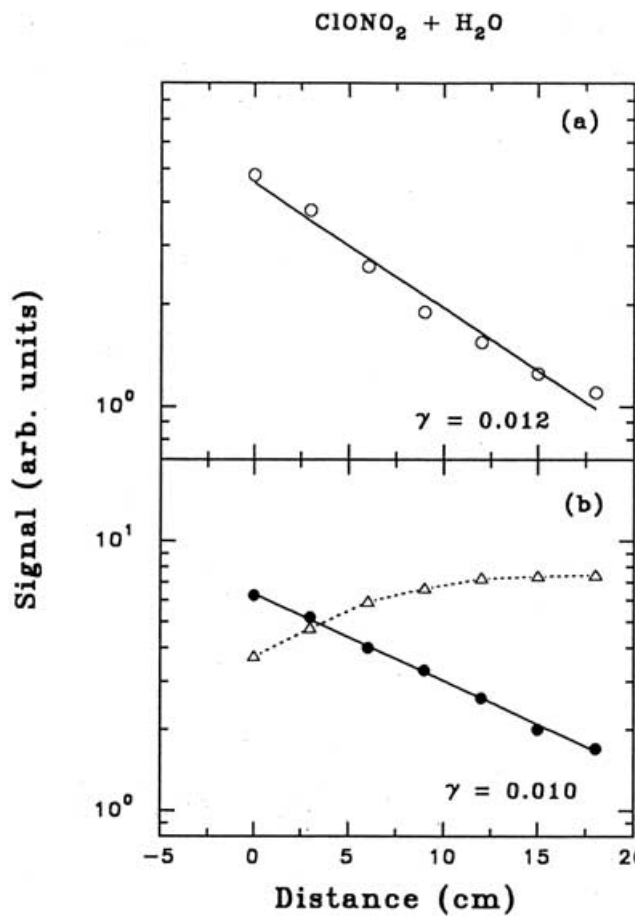

Figure 8. $ClONO_2$ and HOCl signals as a function of injector positions (or reaction times): (*a*) $ClONO_2$ decay; (*b*) HOCl growth.

3.1.1. *$ClONO_2 + H_2O$*

Both the electron-impact ionization mass spectrometer and the CIMS were used in these studies [25, 26]. As discussed in section 2, we used a sliding injector to admit the reactant gases, for example $ClONO_2$, into the wall-coated reactor. The injector controlled the exposure time for the interaction between gases and liquid H_2SO_4. One of the examples is shown in figure 7. The data indicate the removal of $ClONO_2$ and the appearance of the HOCl product. The other product, HNO_3, was not desorbed from the film since it is very soluble in the cold H_2SO_4 solution. The reaction probability (γ) for reaction (5) was determined from the decay rate of $ClONO_2$ and the appearance rate of HOCl as shown in figure 8. We obtained essentially the same γ values from these measurements within the experimental error limits.

By holding the water vapour pressure constant at 3.8×10^{-4} Torr and varying the reactor temperatures from 196 to 220 K, we were able to change the acid composition from $\sim$48 to 70 wt%. The data are shown in figure 9. The open circle data were obtained from the loss rates of $ClONO_2$ while the full circle data are from the growth rates of HOCl. The full curve is a polynomial fit

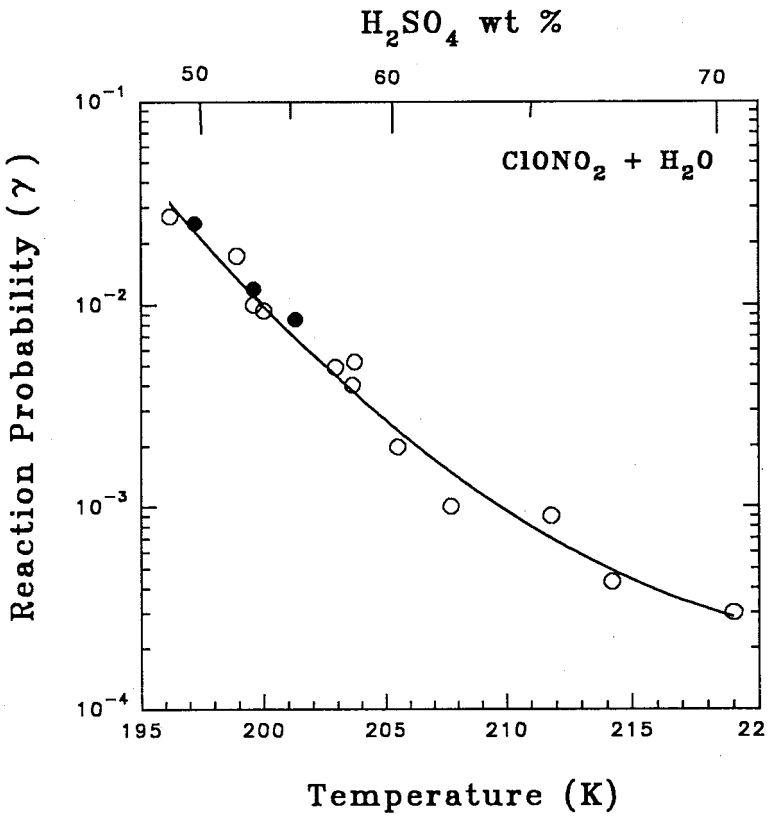

Figure 9. Reaction probability for $ClONO_2$ hydrolysis versus temperature on liquid H_2SO_4 films at a constant $P(H_2O) = 3.8 \times 10^{-4}$ Torr. The open circles indicate the data from the decay of $ClONO_2$ and the full circles show the data from the growth of HOCl.

($\log \gamma = a_1 + a_2 T + a_3 T^2$) through the data [25]. As the temperature varied from 220 to 196 K (or acid composition from 70 to 48 wt %), the values were found to vary steeply from 3×10^{-4} to ~ 0.03. This suggests that the hydrolysis rates depend on the amount of water in the solutions.

It has recently been suggested that type I PSCs may be a ternary solution of containing HNO_3, H_2SO_4 and H_2O. By adding a constant HNO_3 vapour pressure of 5×10^{-7} Torr, a typical vapour pressure in the lower stratosphere, we obtained γ values almost identical to those determined in the binary solution. These data are shown in figure 10. Open circles are the data with HNO_3 vapour and the full curve represents the binary solution data. The effect of HNO_3 vapour on the reactivity appeared to be negligible [26].

Our results agree well with other values compiled in the NASA Panel Report [5] and IUPAC evaluation [6].

3.1.2. $N_2O_5 + H_2O$

Two independent studies were used to investigate this reaction. The first study used the wall-coated reactor at lower temperature to mimic the atmospheric conditions in the upper troposphere and lower stratosphere [26]. In the second

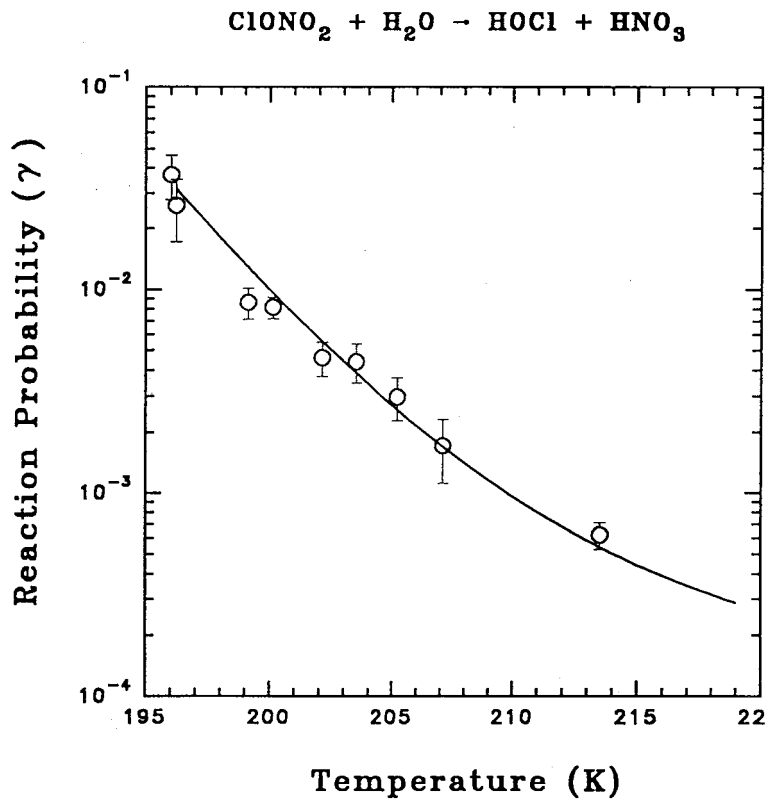

Figure 10. Comparison of reaction probability for $ClONO_2$ hydrolysis either in the presence (open circles) or in the absence (full curve) of $P(HNO_3) = 5.0 \times 10^{-7}$ Torr. The difference appears to be minimal.

study we used an aerosol reactor at 294 K to represent the average temperature in the global troposphere [33]. Chemical ionization mass spectrometry was used for these studies.

The results of the wall-coated reactor study are shown in figure 11 (*a*). The γ values in the binary solutions are very large, ~ 0.1, in the temperature range from 195 K ($\sim$46 wt%) to 227 K ($\sim$75 wt%). However, by adding a known HNO_3 vapour pressure of $\sim 5 \times 10^{-7}$ Torr into the reactor, the reactivity was significantly reduced. Figure 11 (*b*) shows the data with $P(H_2O) = 1 \times 10^{-3}$ Torr and figure 11(*c*) with $P(H_2O) = 3.8 \times 10^{-4}$ Torr.

As shown in figure 11, the uptake coefficient of N_2O_5 hydrolysis on the HNO_3-rich ternary solution was about a factor of 5 smaller than that on an H_2SO_4 surface free of HNO_3. The reduced reactivity with increasing HNO_3 appeared to reflect the nature of the reaction mechanism, which suggests the limitation by an ionic equilibrium [51, 52],

$$N_2O_5(aq) \leftrightarrow NO_2^+(aq) + NO_3^-(aq). \tag{23}$$

HNO_3 dissolved in H_2SO_4 acid also dissociated to yield NO_3^-, thus potentially suppressing the dissociation of N_2O_5 and resulting in a lower solubility of N_2O_5 in the H_2SO_4–HNO_3–H_2O ternary solution.

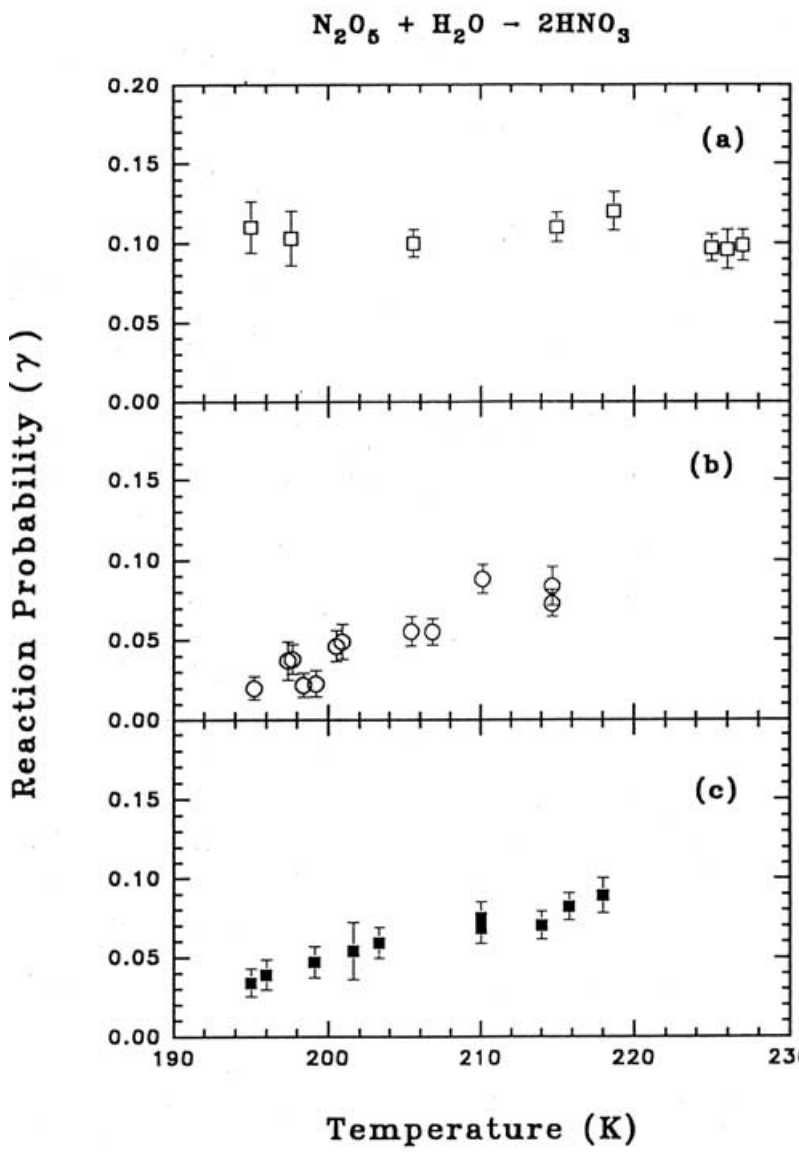

Figure 11. Reaction probability of N_2O_5 with H_2O as a function of temperature (*a*) without and (*b*) and (*c*) with $P(HNO_3) = 5.0 \times 10^{-7}$ Torr. $P(H_2O) = 3.8 \times 10^{-4}$ Torr in (*a*) and (*c*) and 1.0×10^3 Torr in (*b*).

The reactive uptake on H_2SO_4 aerosols had been examined extensively by a number of groups previously [45, 51–57], and thus our examination was kept quite limited, mainly for the confirmation of these previous results using our apparatus. The data are shown in figure 12. Our data correspond reasonably well published values [45, 51–57] of N_2O_5 uptake at lower relative humidity (RH < 25%). If we exclude the data (shown by open circles) of Mozurkewich and Calvert [51] because the data analysis is in error [53], we derive a fit for all data by linear regression:

$$\gamma[H_2SO_4] = 0.052 - 2.79 \times 10^{-4} \times \mathrm{RH}. \tag{24}$$

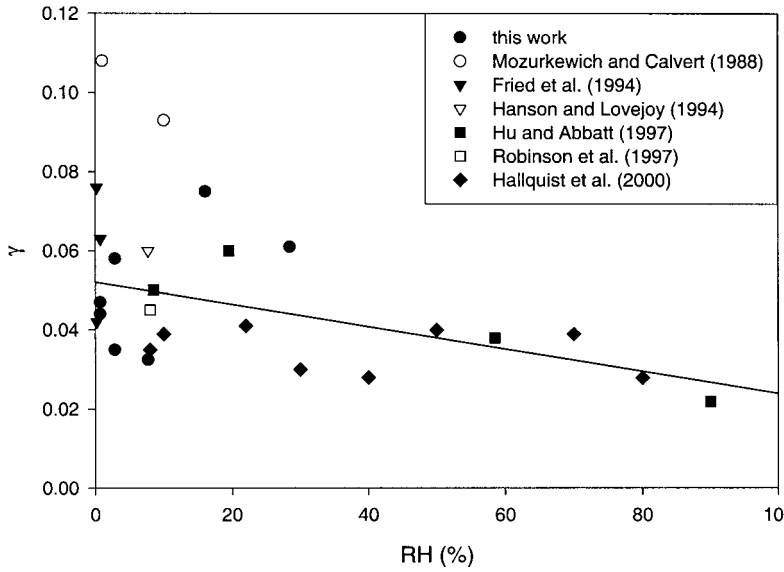

Figure 12. Comparison of reaction probability measurements for N_2O_5 hydrolysis on H_2SO_4 aerosols as a function of relative humidity (or acid composition) at 295 K.

The reaction probability on H_2SO_4 aerosol shows only a weak dependence on the relative humidity, in contrast to those on ammonium-containing aerosols as shown in the following sections. The results reported here suggest that the reaction mechanism in the uptake of N_2O_5 by these sulphate aerosols is substantially different. We will discuss this subject later in this section.

3.1.3. *$ClONO_2 + HCl$*

Results of γ measurements on liquid H_2SO_4 films are shown in figure 13 as a function of temperature. The open and full circles correspond to those determined from $ClONO_2$ decay and Cl_2 growth respectively. The top axis labels the amount of H_2SO_4 (wt%) estimated from the H_2O vapour pressures in H_2SO_4 solutions [44, 58]. In these experiments, the HCl partial pressures fluctuated only slightly in the range $(3–4) \times 10^{-7}$ Torr, and the initial partial pressures of HCl were always higher than those of $ClONO_2$ so that the pseudo-first-order assumption applied ($P_{ClONO_2} = 8 \times 10^{-8}–2 \times 10^{-7}$ Torr). The uncertainties in the γ values were approximately $\pm 30\%$ for $\gamma_2 < 0.1$. For larger γ values approaching ~ 0.3 (which are more sensitive to the gas-phase diffusion) the uncertainties were as large as a factor of 3 or 4. Some scatter in γ was also related to variation in HCl partial pressures during the various experiments; a P_{HCl} variation of $(3–4) \times 10^{-7}$ rendered about a 20% difference in γ, according to figure 13.

In figure 13, γ approached ~ 0.3 at 195 K, whereas the value at 212 K was more than two orders of magnitude smaller. This profound temperature dependence appeared to be correlated with the amount of dissolved HCl in the film: at a fixed P_{H_2O} of 3.8×10^{-4} Torr, HCl solubility in H_2SO_4 increases by about three orders of magnitude over the temperature range from 210 to 195 K [5, 6]. As explained above, this solubility behaviour was caused jointly by the changing temperature and changing H_2SO_4 content, when P_{H_2O} was held constant.

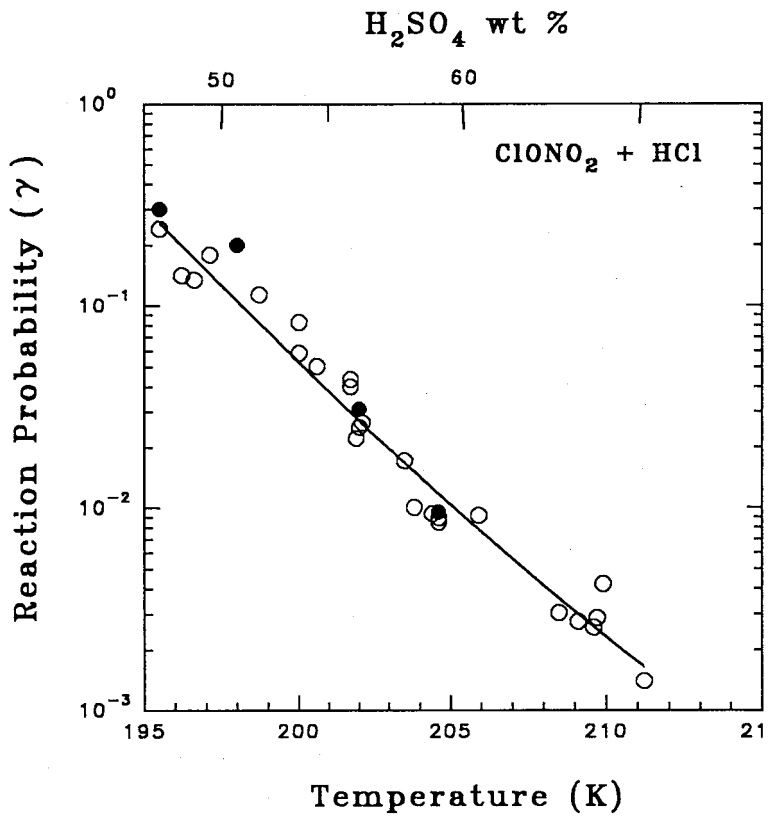

Figure 13. Reaction probability measurements of $ClONO_2$ with HCl on liquid H_2SO_4 films as a function of temperature at $P(H_2O) = 3.8 \times 10^{-4}$ Torr. The open and full circles are the data for $ClONO_2$ decay and Cl_2 growth respectively.

We also investigated this reaction in the ternary solution of H_2SO_4–HNO_3–H_2O. The reactivity appeared to be independent of the presence of HNO_3 vapour at about 5×10^{-7} Torr at 200 K [26].

3.1.4. *HOCl + HCl*

Reaction probability (γ) measurements between HOCl and HCl were conducted in the same manner as those for the reaction of $ClONO_2$ with HCl. As stated previously, HOCl also physically dissolves in H_2SO_4 solutions. To quantify better the potential effect on the reaction probability of HOCl dissolving in the film, we determined γ both from HOCl decay and from Cl_2 rise. The temperature dependence of the reaction of HOCl with HCl is illustrated in figure 14 using HOCl partial pressures of 9×10^{-8}–1×10^{-7} Torr. The HCl partial pressure was maintained at $(3–4) \times 10^{-7}$ Torr.

Reaction probabilities of HOCl with HCl are in general larger than those measured for $ClONO_2$ reacting with HCl (figure 13) by a factor of 3–7. For example, γ is greater than 0.3 at 197 K and decreases to about 0.004 at 215 K. It should be noted that the Henry's law solubility coefficient for HOCl is about an order of magnitude greater than that for HCl under the same conditions [25]. The mechanism

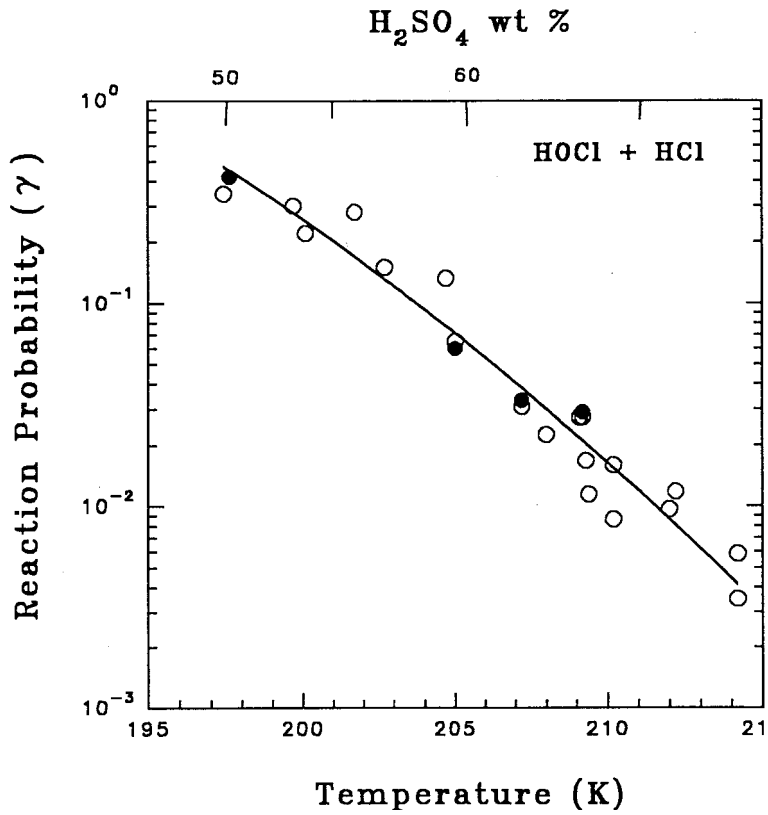

Figure 14. Reaction probability measurements of HOCl with HCl on liquid H_2SO_4 films as a function of temperature at $P(H_2O) = 3.8 \times 10^{-4}$ Torr. The open and full circles are the data for HOCl decay and Cl_2 growth respectively.

for the reaction of HOCl with HCl is likely to be acid-based catalysis, occurring after the uptake and subsequent solvation of both species:

$$H^+Cl^-(aq) + H^+ClO^-(aq) \rightarrow Cl_2(g) + H_2O(aq). \quad (25)$$

Eigen and Kustin [59] previously investigated reaction (25) in aqueous phase at room temperature. It was found that the rate is limited by liquid-phase diffusion.

We also checked the effect of an HNO_3 vapour pressure of 5×10^{-7} Torr at 200 K. The difference between the binary solution and the ternary solution appears to be negligible within the error limits. The result was similar to that of the reaction between $ClONO_2$ and HCl as discussed in the preceding section.

3.1.5. *HONO uptake and HONO + HCl*

HONO is produced by combustion emission from aircraft engines operating in the upper troposphere. Arnold *et al.* [60] reported *in situ* measurements of trace species inside a DC-9 contrail around 10 km: the measured HONO concentrations inside the DC-9 plume were $\sim 5 \times 10^9$ molecules cm^{-3}, about two orders of magnitude higher than the background values. In addition, sulphuric acid aerosols nucleate homogeneously inside aircraft plumes owing to SO_2 emissions. *In situ* aerosol measurements of Concorde supersonic aircraft plumes confirmed the exist-

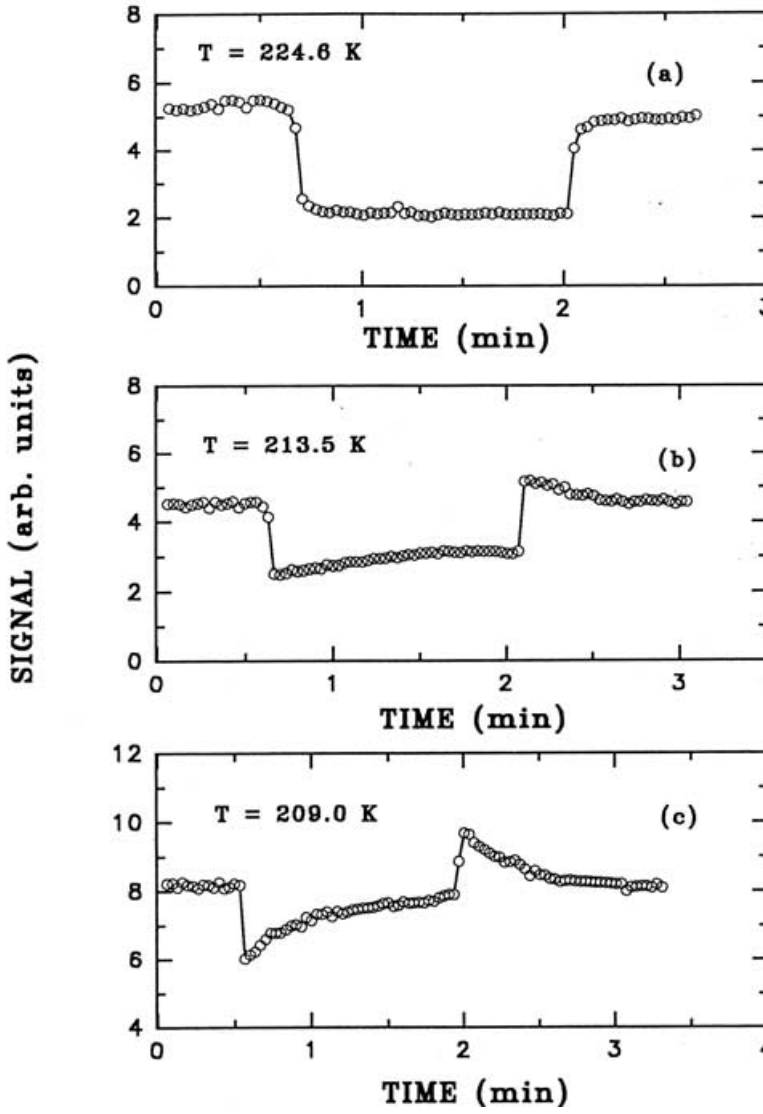

Figure 15. Variation of HONO signals as it was exposed and not exposed to 5 cm length of (*a*) 72 wt% H_2SO_4 at 224.6 K, (*b*) 65 wt% H_2SO_4 at 213.5 K and (*c*) 61 wt% H_2SO_4 at 209.0 K.

ence of high aerosol densities inside aircraft plumes, with particles most likely consisting of 70–80 wt% H_2SO_4 [61]. Hence, heterogeneous processes involving HONO on H_2SO_4 particles may influence plume chemistry, particularly in terms of hydrogen oxides HO_x, OH and HO_2.

The first phase of the study involves the uptake of HONO in H_2SO_4. Figure 15 shows the data for acid compositions of 72, 65 and 61 wt%. The kinetic behaviour indicates the shift of uptake mechanisms from reaction to solvation (from 72 to 61 wt%). Thus, the measured uptake coefficient (γ) of HONO in H_2SO_4 increased with increasing acid content forming nitrosyl sulphuric acid, $NOHSO_4$ [62, 63]. In concentrated solutions (> 70 wt% H_2SO_4), HONO underwent irreversible aqueous

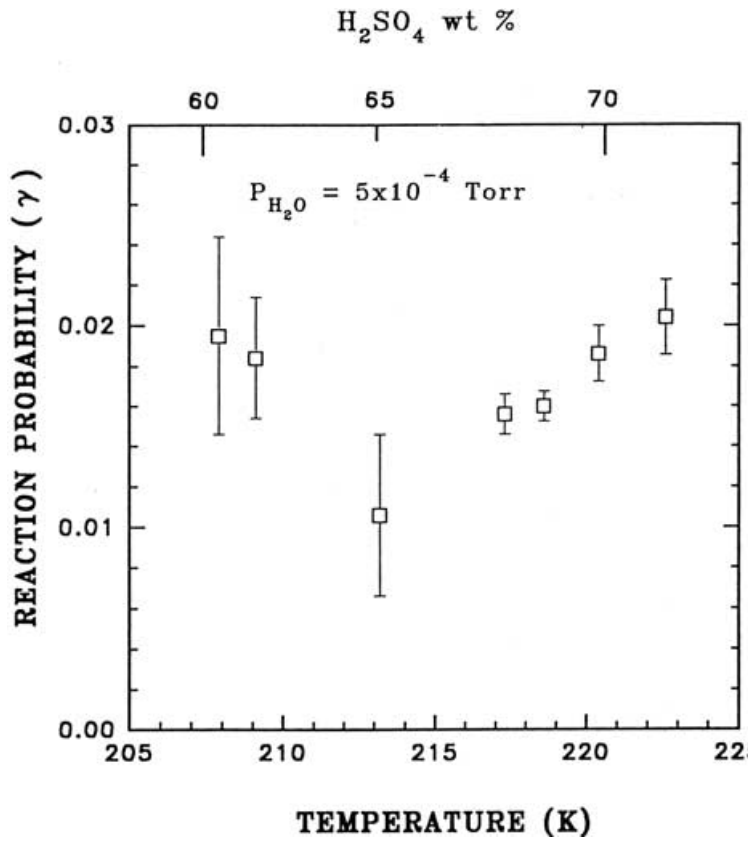

Figure 16. Reaction probability (γ) of HCl with HONO dissolved in H_2SO_4. The reaction probability was obtained from the observed HCl decay rate, when HCl was exposed to HONO-doped sulphuric acid.

phase reaction with an uptake coefficient of about 0.07. The dependence of γ on the acid composition is in good agreement with recent measurements [64–66].

In 1996 we proposed a new mechanism of chlorine activation involving the reaction of HCl with HONO,

$$HCl + HONO \rightarrow H_2O + NOCl, \quad (27)$$

in liquid H_2SO_4 at conditions that prevail in the stratosphere [27]. In figure 16, it can be observed that HCl reacts with HONO dissolved in sulphuric acid ($\gamma = 0.01$–0.02), releasing gaseous nitrosyl chloride (NOCl). In the stratosphere, ClNO photodissociates rapidly to yield atomic chlorine, which destroys ozone through catalytic chain reactions. The reaction of HCl with HONO on sulphate aerosols may affect stratospheric ozone balance during the elevated H_2SO_4 loading after volcanic eruptions or due to the emission from the projected High-Speed Civil Transport.

3.1.6. *Comparison of uptake coefficients for $ClONO_2$, N_2O_5 and HONO*

It is intriguing to compare the γ value of HONO with those of $ClONO_2$ and N_2O_5 as a function of temperature (or acid composition). These results are shown in figure 17.

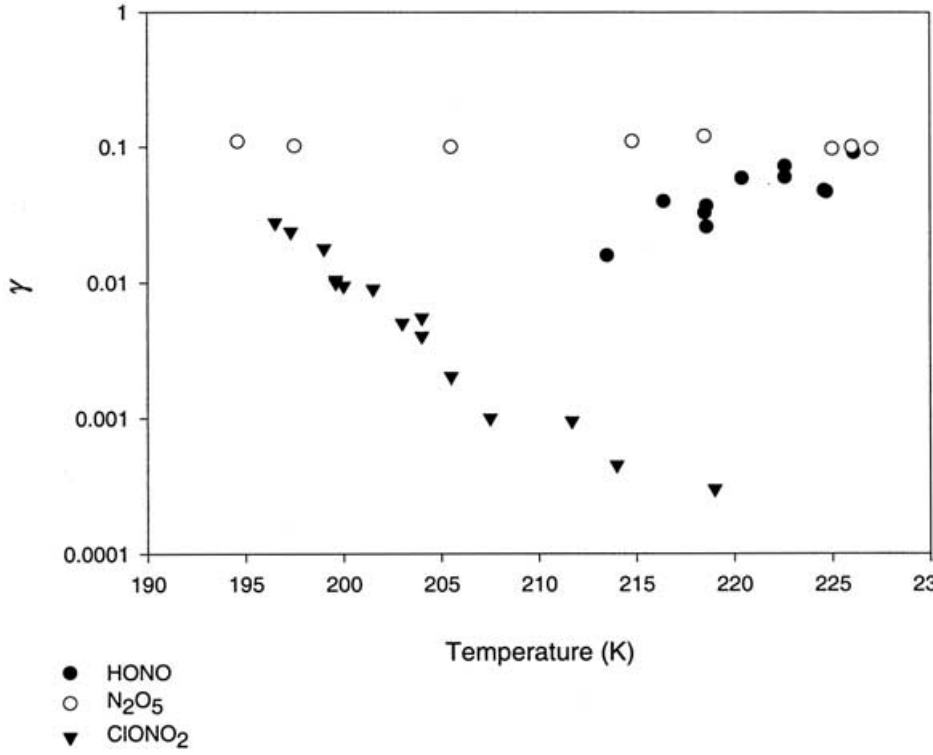

Figure 17. Comparison of uptake coefficients for N_2O_5, HONO and $ClONO_2$ in liquid H_2SO_4.

It was previously realized that equilibrium of N(+III) species in highly acidic H_2SO_4 at room temperature may involve complex aqueous reactions between nitrogen species and H_2SO_4. Deschamps [63] reported absorption spectra between 214 and 300 nm for 70–96 wt% H_2SO_4 containing 1 mol l^{-1} dissolved $NO^+HSO_4^-$. The spectrum showed only the nitrosonium ion (NO^+) in 96 wt% H_2SO_4; the amounts of H_2ONO^+ (hydrated nitrosonium ion) and NO^+ were equal in 88 wt% H_2SO_4; H_2ONO^+ dominated in 70.5 wt% H_2SO_4, with a trace amount of HONO but no NO^+. The proposed ionic mechanism is [62, 63]

$$HONO + H_2SO_4 \rightleftarrows NO^+HSO_4^- + H_2O, \tag{28}$$

$$NO^+HSO_4^- \rightleftarrows NO^+ + HSO_4^-, \tag{29}$$

$$NO^+ + H_2O \rightleftarrows H_2ONO^+, \tag{30}$$

$$H_2ONO^+ + H_2O \rightleftarrows H_3O^+ + HONO. \tag{31}$$

$NO^+HSO_4^-$ is an ionic species soluble in H_2SO_4. In concentrated sulphuric acid, $NO^+HSO_4^-$ accumulates in the liquid and, on reaching saturation, precipitates out as solid crystals to permit further accumulation.

However, $ClONO_2$ or N_2O_5 may proceed through both hydrolysis and ionic chain reactions, for example

$$XONO_2 + H_2O \rightarrow XOH + HNO_3, \quad (32)$$

$$XONO_2 + H^+ \rightarrow XOH + NO_2^+, \quad (33)$$

$$NO_2^+ + H_2O \rightarrow HNO_3 + H^+. \quad (34)$$

Robinson *et al.* [45] have recently developed a theoretical model by incorporating liquid-phase diffusion, solubility and chemical reactions. Their model results agree very well with our measurements of N_2O_5 hydrolysis as shown in figure 6 of their article [45]. In addition, in a very recent study Shi *et al.* [67] also compared their model results with our data on $ClONO_2$ hydrolysis and they found a good agreement between theory and measurement (figure 2 in their paper).

3.1.7. *Comparison of reaction probabilities for HCl with $ClONO_2$, HOCl and HONO*

Results for reactions (3), (4) and (27) are summarized in figure 18. These reactions have a similar mechanism because all of them form Cl_2 as products. While reactions (3) and (4) proceed at much higher rates in cold and dilute solutions, reaction (27) favours a faster rate at concentrated solutions. The reaction mechanism between HCl and HONO dissolved in sulphuric acid may also vary with the acid composition, depending on the N(+III) species available in the liquid. Hence, it is likely that HCl reacts with the hydrated nitrosonium ion in dilute solutions

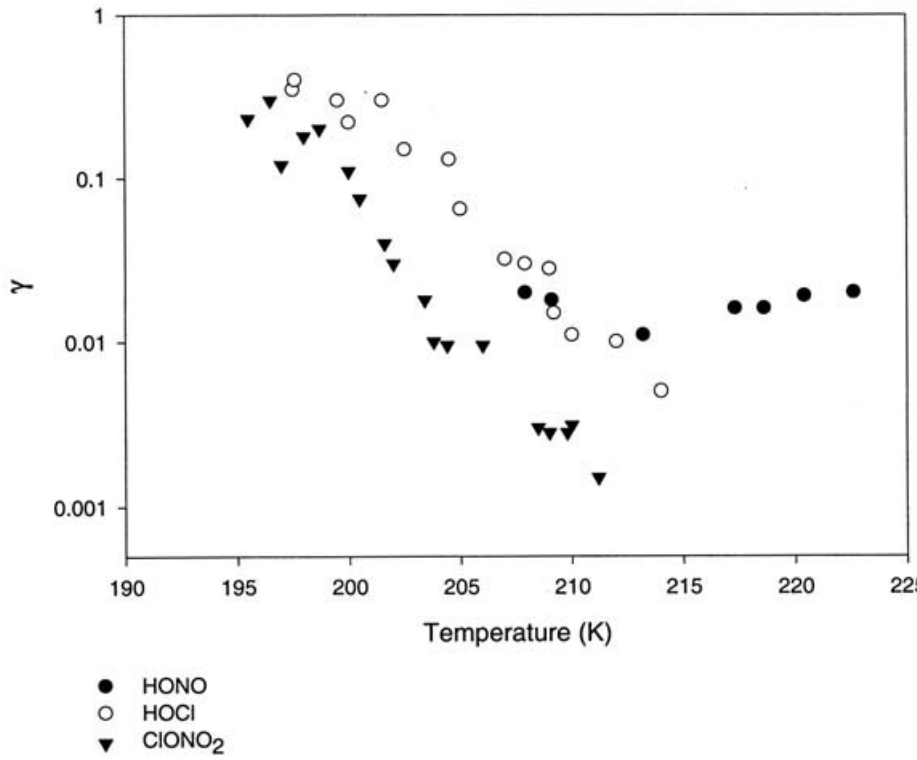

Figure 18. Comparison of reaction probabilities for the reactions of HCl with HOCl, HONO and $ClONO_2$ in liquid H_2SO_4.

$$HCl + H_2ONO^+ \rightarrow H_3O^+ + ClNO \tag{35}$$

but with $NO^+HSO_4^-$ in concentrated solutions

$$HCl + NO^+HSO_4^- \rightarrow H_2SO_4 + ClNO \tag{36}$$

Also, at least for the case in concentrated H_2SO_4 (> 70 wt%), the reaction between HCl and HONO dissolved in sulphuric acid occurs very near the gas–liquid interface, owing to exceedingly small HCl solubility.

Very recently, Shi *et al*. [67] suggested that a complex ionic mechanism

$$HCl + HClONO_2^+ \rightarrow HNO_3 + Cl_2 + H^+ \tag{37}$$

$$HCl + H_2OCl^+ \rightarrow H_3O^+ + Cl_2 \tag{38}$$

may be involved in reactions (3) and (4) and further developed a model to compare with our measurements. There is a reasonable agreement between model and many laboratory measurements [5, 6]. Details have been given in their article [67] and will not be repeated here.

3.1.8. *HO_2NO_2 (PNA)*

PNA is a powerful oxidant and is present in the atmosphere at very low concentrations (< 1 part per billion in volume). PNA is formed through a termolecular reaction of HO_2 with NO_2 and is intricately linked to NO_x and HO_x. The major sinks for PNA include thermal decomposition, photodissociation and reaction with OH radicals [68]. In addition, both PAN and PNA may interact with sulphate aerosols in which they can affect their gas–particle partitioning. We have also measured an effective Henry's law constant for these two species in H_2SO_4. Furthermore, we have investigated the reaction pathway $HO_2NO_2 \rightarrow HONO + O_2$. Photolysis of HONO may be one of the important sources of hydroxyl radicals in the atmosphere.

The interaction of PNA vapour with liquid H_2SO_4 was investigated for acid contents ranging from 53 to 74 wt% and at temperatures between 205 and 230 K, using a fast flow-reactor coupled to a CIMS. PNA was physically taken up by liquid H_2SO_4, without undergoing irreversible aqueous phase reactions. From the time-dependent uptake, the quantity $H^*(D_l)^{1/2}$ (that is, the product of the effective Henry's law solubility constant and the square root of the liquid-phase diffusion coefficient) was obtained. The effective Henry's law solubility constant H^* of PNA in liquid H_2SO_4,

$$\ln(H^*) = 3.69 - m_{H_2SO_4}(-0.25 + 65/T) - 8400\,(1/T_0 - 1/T), \tag{39}$$

for PNA [28, 69] where $m_{H_2SO_4}$ is the molality of H_2SO_4, T is temperature and $T_0 = 298.15$ K. The data are plotted in figure 19. The H^* values were derived by estimating the liquid-phase diffusion coefficient on the basis of a cubic cell model. In general, the solubility was found to increase with decreasing acid content and decreasing temperature. The measured solubility reveals that PNA should exist predominantly in the gas phase under conditions characteristic of the mid- or lower-latitude stratosphere. For winter polar stratospheric conditions, however, incorporation of PNA into sulphate aerosols may lead to redistribution of PNA from the gas to condensed phases, potentially affecting stratospheric HO_x and NO_x concentrations.

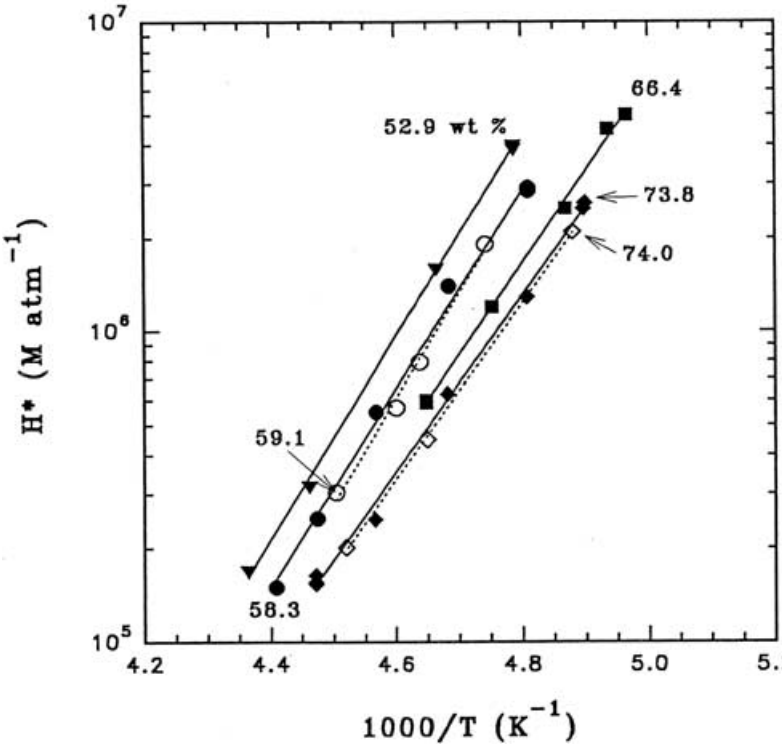

Figure 19. The effective Henry's law constants of PNA in liquid H_2SO_4.

3.1.9. *$CH_3CO(O_2)NO_2$ (PAN)*

PAN has been identified as important reservoir species for reactive nitrogen-containing compounds (NO_y) [68]. Recent atmospheric measurements have revealed significant concentrations (up to 0.3 ppb) of PAN in the atmosphere [70]. In the upper troposphere and lower stratosphere PAN is formed primarily by the associative reaction of the peroxyacetyl radical ($CH_3C(O)O_2$) with NO_2. PAN is relatively stable in the lower stratosphere, and its main sinks include thermal deposition, ultraviolet photolysis and reactions with atomic chlorine or hydroxyl radicals (OH) [68]. PAN can be transported throughout the atmosphere by wind circulation, providing a source of NO_x in the free troposphere where it is critical to the formation of ozone and the oxidation of hydrocarbons.

Henry's law constants for PAN in water near room temperature, literature values for the associative enthalpy change and solubilities of PAN and PNA in aqueous H_2SO_4 (46–74 wt%) at temperatures relevant to the stratosphere ($T = 200$–230 K) are found to be thermodynamically consistent and are used to determine the effective Henry's law constants (in units of mol kg^{-1} atm-1^{-1}),

$$\ln(H^*) = 1.07 - m_{H_2SO_4}(0.69 - 152/T) - 5810(1/T_0 - 1/T), \qquad (40)$$

for PAN [29, 69] where $m_{H_2SO_4}$ is the molality of H_2SO_4, T is temperature and $T_0 = 298.15$ K. The results are plotted in figure 20. To a first-order approximation, the activity coefficients of PAN and PNA in aqueous H_2SO_4 are found to have a simple Setchenow-type dependence on H_2SO_4 molality.

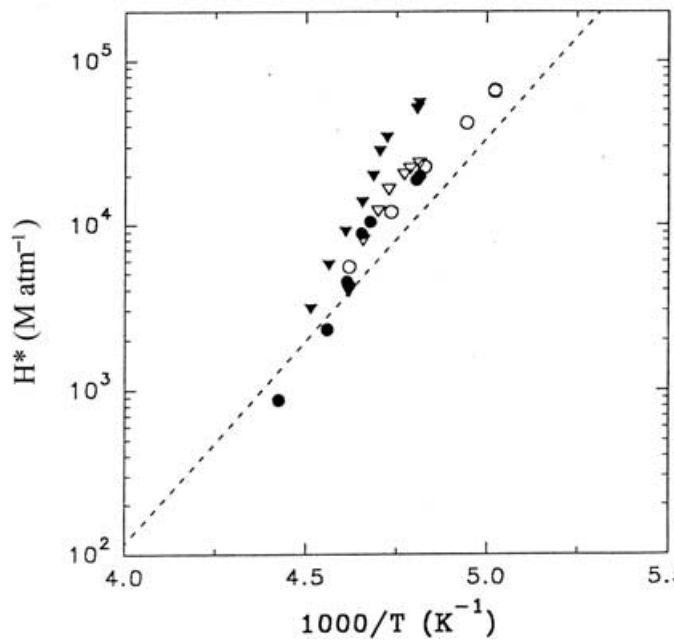

Figure 20. The effective Henry's law constants of PAN in liquid H_2SO_4. The different symbols correspond to different H_2SO_4 contents: 46 wt% (open circles), 54 wt% (full circles), 59 wt% (open triangles) and 72 wt% (full triangles). The broken line represents Henry's solubility constants extrapolated to low temperatures based on the work of Kame *et al.* [71] and Kame and Schurath [72].

3.1.10. *Acetone (CH_3COCH_3)*

In the atmosphere photolysis products of acetone, such as methylperoxy and peroxyacetyl radicals, contribute to the formation of odd hydrogen species (HO_x) as well as PAN through reaction with nitrogen oxides [71]. In affecting the concentrations of atmospherically important species (HO_x and NO_x), acetone can significantly influence ozone formation, especially at altitudes in the upper troposphere where it is perhaps the primary source of HO_x [72–76]. Sources of acetone in the atmosphere include secondary reactions of hydrocarbons (the largest source), biomass burning and direct biogenic and anthropogenic emissions. Since acetone appears to be a significant trace gas species with a budget of as much as 0.5–1.0 ppb in the atmosphere [77], it is important to understand homogeneous and heterogeneous processes that influence the amount of available acetone. Although acetone is quite soluble in water, $H \approx 30\,\mathrm{M\,atm^{-1}}$ at 298 K [78–82], its partition coefficient strongly favours the gas phase and thus it appears that direct removal by water droplets or rainwater in the upper troposphere may not be a significant sink of acetone [83–85].

The uptake of acetone vapour by liquid sulphuric acid has been investigated over the range from 40 to 87 wt% H_2SO_4 and between the temperatures of 198 and 300 K. Studies were performed with a flow-tube reactor, using a QMS for detection. At most concentrations studied (40–75 wt%), acetone was physically absorbed by H_2SO_4 without undergoing irreversible reaction. However, at acid concentrations at or above 80 wt%, reactive uptake of acetone was observed, leading to products such as mesityl oxide and/or mesitylene. From time-dependent uptake data and liquid-phase diffusion coefficients calculated from molecular viscosity, the effective

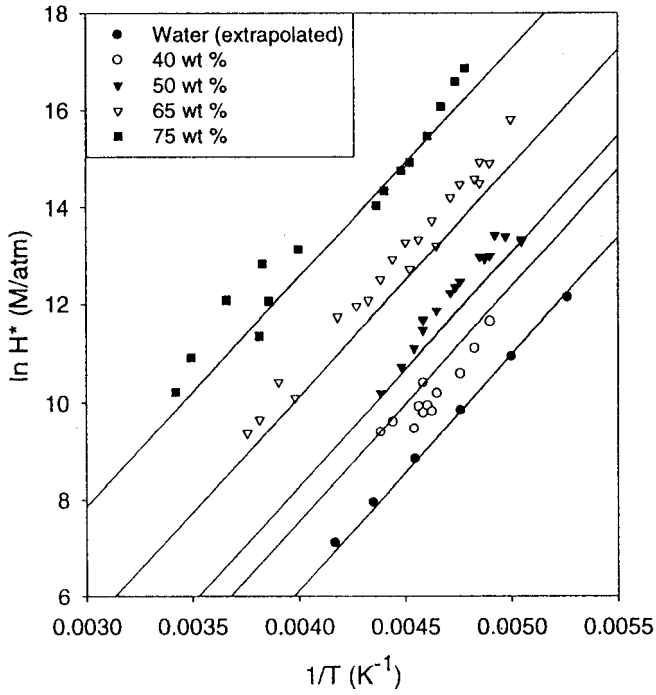

Figure 21. The effective Henry's law constants of acetone in liquid H_2SO_4.

Henry's law solubility constant (H^*) was determined and is shown in figure 21. The solubility of acetone in liquid H_2SO_4 was found to increase with increasing acid concentration and decreasing temperature. This value suggests that acetone primarily remains in the gas phase rather than absorbing into sulphate aerosols under atmospheric conditions.

In order to express acetone solubility as a function of temperature and H_2SO_4 concentration, we use a Setchenow equation [30, 70, 86]:

$$\ln(H^*) = \ln(K_{H(T_0)}) - m_{H_2SO_4} f + (\Delta H_0/R)(1/T_0 - 1/T) \tag{41}$$

where $\ln(K_{H(T_0)}) = 3.00$, $\Delta H_0/R = -4850\,\mathrm{K}$, $T_0 = 298.15\,\mathrm{K}$, $m_{H_2SO_4}$ is the molality of H_2SO_4 and $f = -0.23 + 5.0/T$. The first and third terms relate to the solubility of acetone in water while the second term directly expresses the contribution of H_2SO_4. The results are in good agreement with those obtained by Klassen *et al.* [87] and Imamura and Akiyoshi [88].

The results with acid compositions greater than 80 wt% suggest that mesityl oxide and/or mesitylene is formed when acetone interacts with liquid H_2SO_4 [89–91]. The reaction mechanism is depicted in figure 22. In principle, an acetone dimer reaction in H_2SO_4 forms mesityl oxide while the trimer reaction produces mesitylene. These results are consistent with those reported in previous investigations [89–91].

3.1.11. *Methanol and ethanol*

Both methanol and ethanol were also observed in the upper troposphere, but with the mixing ratios somewhat less than that of acetone [70]. As a series of laboratory studies, we are investigating the interaction of these oxygenated hydro-

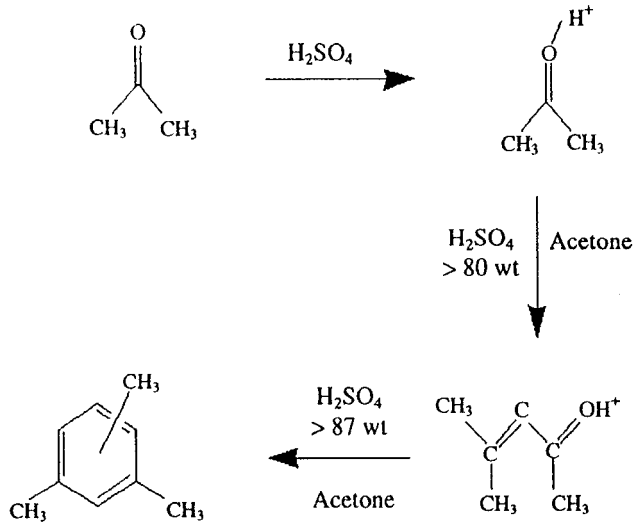

Figure 22. Schematic of the reaction mechanism for acetone with H_2SO_4 forming mesityl oxide and mesitylene (or trimethylbenzene) at various concentrations.

carbons with liquid H_2SO_4 [30]. These studies may help to explain recent observations of mixed sulphate–organic aerosols in the upper troposphere by a laser ionization particle spectrometer [92].

The uptake of gas-phase methanol by liquid H_2SO_4 has been investigated over the composition range of 40 to 85 wt% H_2SO_4 and between the temperatures of 210 and 235 K [31]. Laboratory studies were performed with a flow-tube reactor coupled to an electron-impact ionization mass spectrometer for detection of trace gases. While reversible uptake was the primary mechanism at low acid concentrations and higher temperatures, irreversible reaction between methanol and concentrated H_2SO_4, forming methyl hydrogen sulphate (CH_3HSO_4) and dimethyl sulphate ($(CH_3)_2SO_4$), was observed. We have obtained uptake coefficients $\gamma \sim 0.01$–0.02 for acid compositions of 65–80 wt% (figure 23). The results suggest that the reaction with H_2SO_4 forming CH_3HSO_4 and $(CH_3)_2SO_4$ is the dominant loss mechanism of methanol and the oxidation of methanol is only a minor source of hydroxyl radicals in the upper troposphere.

Very recent measurements on the uptake of ethanol into liquid H_2SO_4 in our laboratory show a similar dependence of acid composition as the uptake of methanol [32]. This is not unexpected because methanol and ethanol have almost identical physical and chemical properties.

3.2. *Sulphuric acid monohydrate*

Both the phase and the composition of sulphate aerosols are likely to affect their ability to promote heterogeneous reactions. In the laboratory, the reaction probabilities of reactions (3)–(6) on liquid H_2SO_4 have been shown to depend strongly on the acid content: they proceed efficiently in dilute H_2SO_4 solutions at low temperatures [25, 26]. Hence, these reactions occurring on stratospheric sulphate aerosols at high latitudes in winter and early spring could provide important pathways for chlorine activation. Outside of the polar region, the most significant

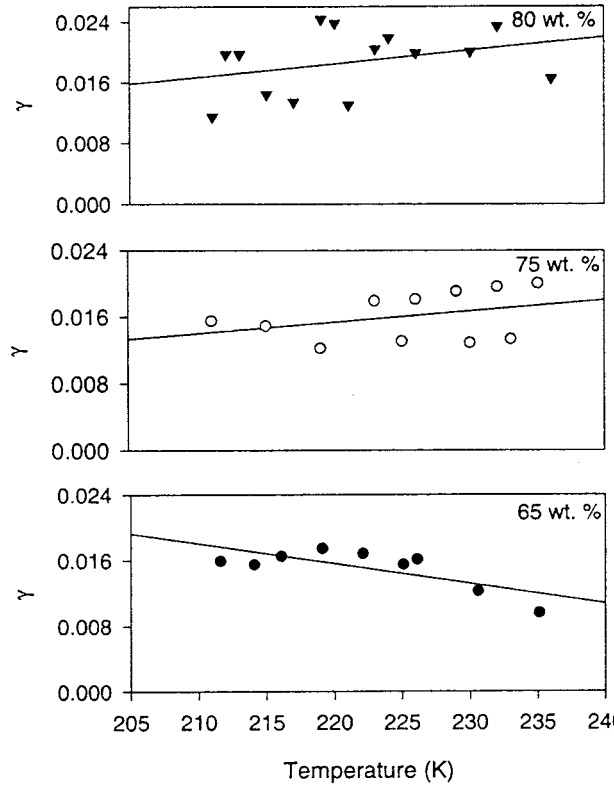

Figure 23. Uptake coefficient measurements for the interaction of gaseous methanol with H_2SO_4 in the range 65–80 wt%.

heterogeneous reaction on the sulphate aerosols is believed to be the hydrolysis of N_2O_5 [6] with the consequent changes in the abundance of various nitrogen and chlorine species. We have also investigated heterogeneous reactions on the surface of SAM.

We have investigated some thermodynamic properties (i.e. freezing and melting points) and heterogeneous chemistry of SAM using a fast flow reactor coupled to an electron-impact ionization mass spectrometer [43]. The freezing point observations show that for H_2SO_4 contents between 75 and 85 wt% the monohydrate crystallizes readily at temperatures between 220 and 240 K (see figure 2). Once formed, SAM can be thermodynamically stable in the H_2O partial pressure range $(1–4) \times 10^{-4}$ Torr and in the temperature range from 220 to 240 K. For a given H_2O partial pressure, SAM melts at lower temperatures. The reaction probability measurements indicate that the hydrolysis of N_2O_5 is significantly suppressed owing to the formation of crystalline SAM: the reaction probability on water-rich SAM is of the order of 10^{-3} at 210 K and decreases by more than an order of magnitude for the acid-rich form. The hydrolysis rate of $ClONO_2$ on water-rich SAM is even smaller, of the order of 10^{-4} at 195 K. No enhancement of these reactions is observed in the presence of HCl vapour at the stratospheric concentrations. The results suggest the possible formation of SAM in some regions of mid- or low-latitude stratosphere and, consequently, much slower heterogeneous reactions on these frozen aerosols.

3.3. $N_2O_5 + H_2O$ on $(NH_4)_2SO_4$ and NH_4HSO_4 aerosols

In a global troposphere model, Dentener and Crutzen [93] have adopted a reaction probability (γ) of 0.1 for reaction (6) on the surface of NH_4HSO_4 aerosol in the atmosphere. They thought that the rate for NH_4HSO_4 is similar to that for liquid H_2SO_4. Dentener and Crutzen found decreases of yearly averaged NO_x, O_3 and OH levels of 49%, 9% and 9% with respect to values obtained by considering gas-phase reactions only. They have also calculated the impact by using a smaller reaction probability of 0.01 and the decreases of NO_x, O_3 and OH are still very high, being 40%, 4% and 3%, respectively. These calculations suggest that the magnitude of γ for reaction (6) on $(NH_4)_2SO_4$ and NH_4HSO_4 aerosols is also of fundamental importance in global tropospheric chemistry.

The uptake coefficients of N_2O_5 on $(NH_4)_2SO_4$ aerosols is shown in figure 24. The uptake on dry aerosols (under the condition of relative humidity less than 40%) is found to be relatively small, < 0.01. As the relative humidity increases above 50%, N_2O_5 uptake increases from ~ 0.01 to ~ 0.04 at 92% relative humidity. The polynomial fit of the data gives

$$\gamma[(NH_4)_2SO_4] = 2.79 \times 10^{-4} + 1.30 \times 10^{-4} \times (RH) - 3.43 \times 10^{-6} \times (RH)^2 + 7.52 \times 10^{-8} \times (RH)^3. \quad (42)$$

Our results are supported by comparison with the phase transition of $(NH_4)_2SO_4$ aerosols described by Tang and Munkelwitz [94] and Xu *et al.* [95]. The aerosol has an efflorescence point near 40% relative humidity at 298 K, above which the water

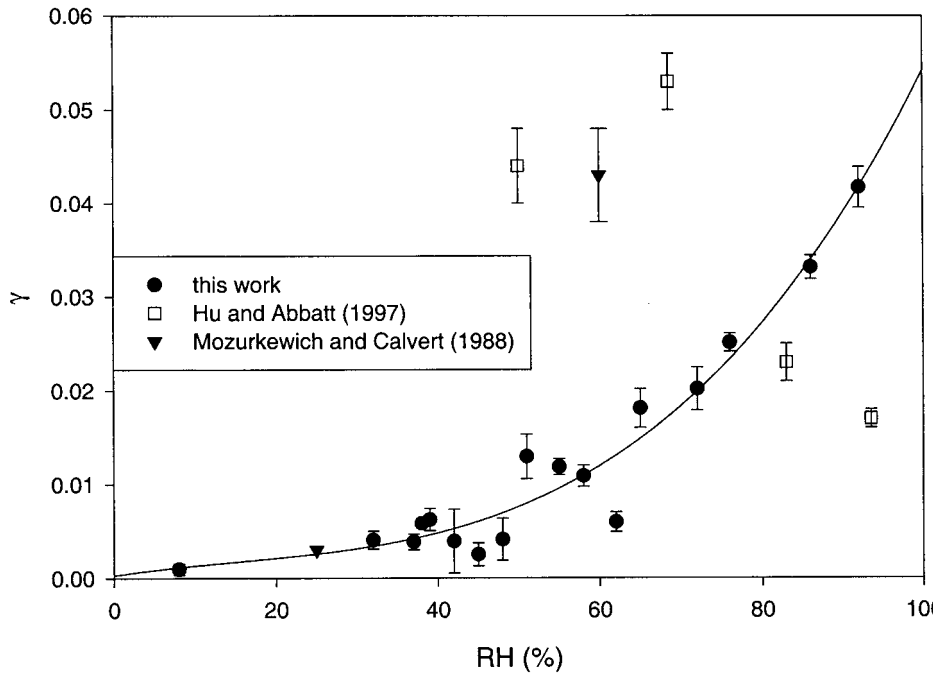

Figure 24. Reaction probability measurements for N_2O_5 hydrolysis on $(NH_4)_2SO_4$ aerosols as a function of relative humidity: full circles [33], open squares [55] and full triangles [51]. The full curve was calculated from a non-linear polynomial fit of our data.

content increases steadily and below which particles are completely dry. As our particles are formed in a wet environment and subsequently dried (measured by the hygrometer), the water content is expected to match these results. It is further noted that the reaction primarily takes place with thin liquid water on the surface of solid aerosols (RH $\leq$ 40%). On the other hand, the hydrolysis may occur throughout the volume of liquid-phase aerosols (RH > 40%) depending on the magnitude of the diffuso-reactive length, $l = (D_l/k_l)^{1/2}$.

In the data treatment we assume the ammonium sulphate aerosols are spherical. At relative humidity greater than 40%, the sulphate aerosols are in liquid form and the assumption is correct. However, under dry conditions (RH < 40%) the aerosols become solid and the crystal structure of ammonium sulphate is orthorhombic. Since the surface area density on the basis of this crystal structure is greater than that using the spherical assumption, the γ values we report in figure 24 may be smaller.

Data for uptake on $(NH_4)_2SO_4$ collected by Hu and Abbatt [55] are represented with open square symbols in figure 24. Our data do not match the trend of these results with relative humidity, but do fall within the same range of γ value (0.02–0.05) at high relative humidity. A limited set of data reported by Mozurkewich and Calvert [51] are also shown in figure 24 (full triangles). Their result at 25% relative humidity is in excellent agreement with out data at low relative humidity. However, their data at 60% relative humidity, needing to be reduced by $\sim$15% because of a small error in the data treatment [53], are still substantially greater than our data.

Experiments similar to the above were also performed for NH_4HSO_4 aerosols. The results are shown in figure 25. The uptake of N_2O_5 increases steadily as the water content increases. Again we use the polynomial fit of our data, and the result is

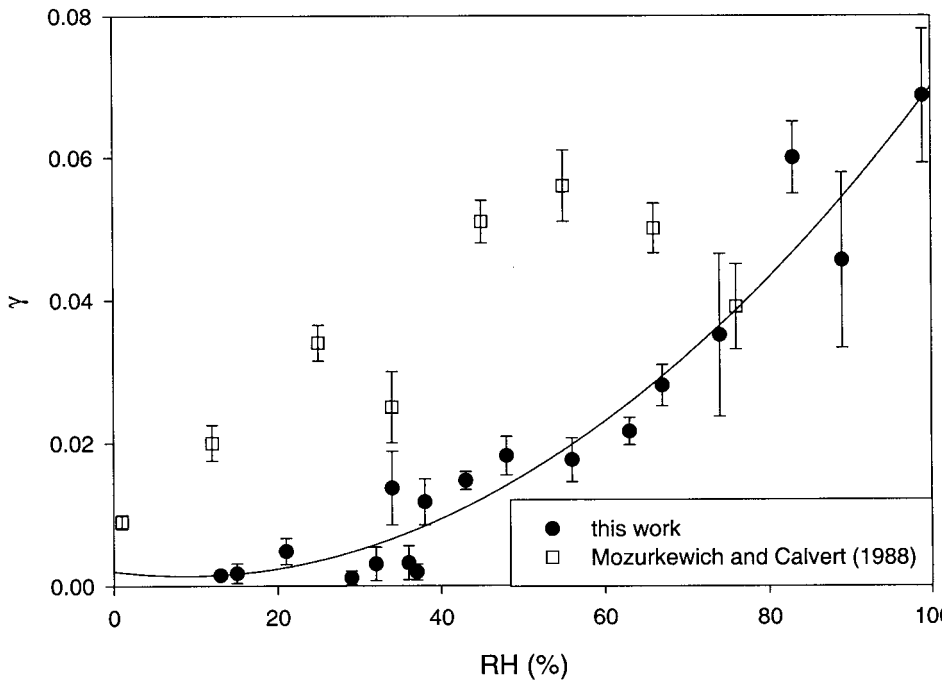

Figure 25. Reaction probability measurements for N_2O_5 hydrolysis on NH_4HSO_4 aerosols as a function of relative humidity: full circles [33] and open squares [51]. The full curve was calculated from a non-linear polynomial fit of our data.

$$\gamma(NH_4HSO_4) = 2.07 \times 10^{-3} - 1.48 \times 10^{-4} \times RH + 8.26 \times 10^{-6} \times (RH)^2. \quad (43)$$

The trend of reaction probability versus relative humidity follows the water activity of the NH_4HSO_4 at room temperature [94–96]. The observation suggests that hydrolysis is the dominant step in the uptake of N_2O_5. A kinetic study was previously investigated at 293 K by Mozurkewich and Calvert [51]. The trend in their data matches ours fairly well, but with somewhat larger γ values overall. It should be noted, however, that subsequent work by this group finds these values should be $\sim$15% smaller [53], which would bring the two studies somewhat closer to agreement. It is also interesting to note that at higher relative humidity (>80%) the γ values appear to approaching that in water ($\sim$0.05) [5].

4. Summary

Over the past decade we have used a flow-tube reactor to investigate the interaction of liquid H_2SO_4 with many trace gases of atmospheric interest. Although these results are rather extensive, we have attempted to summarize our results reported in the preceding sections:

(1) Sulphate aerosols play an important role of atmospheric chemistry, particularly ozone perturbation in the lower stratosphere and upper troposphere due to the release of CFCs and aircraft emissions. The presence of ammonium-containing sulphate aerosols is also critical to the ozone perturbation in the global troposphere.
(2) A fast flow-tube reactor interfaced to a mass spectrometer can provide an accurate measurement of uptake coefficients or reaction probabilities in the range from 1×10^{-4} to $\sim$0.3 under atmospheric conditions.
(3) Both electron-impact ionization and chemical ionization mass spectrometry can monitor trace gas concentration sensitively, in some cases as low as the levels observed in the atmosphere. These spectrometers are complementary in detection selectivity on the basis of different ionization schemes.
(4) The effective Henry's law solubility constant can be accurately measured for both inorganic and organic species in liquid H_2SO_4 in the temperature range from 200 to 300 K and the acid composition range 40–80 wt%. However, it is difficult to maintain a stable acid composition over a longer period of time in warmer environment or more dilute solution.
(5) Reaction product can be easily measured if the solubility of the product is low and the thermal desorption is rapid. However, in many cases, the products remain in the condensed phase, either on the surface or inside the bulk. Spectroscopic methods, such as the sum frequency generation technique, may be useful in identifying reaction mechanisms.
(6) Reactivity on solid substrates, such as SAM, is much smaller than that in liquid solution because the diffusion of trace gas through the substrate is very slow or the acid composition is relatively high.
(7) The experimental approach used in this study has difficulty distinguishing the process occurring on the surface or inside the bulk. The diffuso-reactive length, $l = (D/k)^{1/2}$, calculated from the liquid-phase diffusion and reaction rate, is a useful quantity. If the l value is near the molecular scale (a few nanometres), we can consider that the process is probably occurring on the surface.

(8) An aerosol reactor is complementary to a wall-coated reactor in terms of the temperature and pressure ranges used. We have accurately determined the γ values for reaction (6) using several types of aerosol particle.

Acknowledgments

This research was performed at the Jet Propulsion Laboratory, California Institute of Technology, under a contract with the National Aeronautics and Space Administration (NASA). Helpful discussions of heterogeneous chemistry in liquid sulphuric acid with my colleagues, Francisco Caloz, Sean Kane, Leon Keyser, Raimo Timonen and Renyi Zhang, are sincerely appreciated. The author is also grateful for the reviewer's constructive comments.

References

[1] Molina, M. J., and Rowland, F. S., 1974, *Nature*, **249**, 810.
[2] Johnston, H. S., 1971, *Science*, **173**, 517.
[3] *Scientific Assessment of Ozone Depletion*, 1998, Global Ozone Research and Monitoring Project Report (Geneva: World Meteorological Organization).
[4] *Aviation and the Global Atmosphere*, 1999, Intergovernmental Panel on Climate Change (Cambridge: Cambridge University Press).
[5] (*a*) DeMore, W. B., Sander, S. P., Golden, D. M., Hampson, R. F., Kurylo, M. J., Howard, C. J., Ravishankara, A. R., Kolb, C. E., and Molina, M. J., 1997, *Chemical Kinetics and Photochemical Data for Use in Stratospheric Modeling*, JPL Publication 97-4; (*b*) Sander, S. P., Friedl, R. R., DeMore, W. B., Golden, D. M., Kurylo, M. J., Hampson, R. F., Huie, R. E., Moortgat, G. K., Ravishankara, A. R., Kolb, C. E., and Molina, M. J., 2000, JPL Publication 00-3.
[6] Atkinson, R., Baulch, D. L., Cox, R. A., Crowley, J. N., Hampson, R. F., Kerr, J. A., Rossi, M. J., and Troe, J., 1997, *J. phys. chem. Ref. Data*, **26**, 1329.
[7] Farman, J. C., Gardiner, B. G., and Shanklin, J. D., 1985, *Nature*, **315**, 207.
[8] Solomon, S., Garcia, R. R., Rowland, F. S., and Wuebbles, D. J., 1986, *Nature*, **321**, 755.
[9] Kolb, C. E., Worsnop, D. R., Zahniser, M. S., Davidovits, P., Keyser, L. F., Leu, M. T., Molina, M. J., Hanson, D. R., Ravishankara, A. R., Williams, L. R., and Tolbert, M. A., 1995, in *Progress and Problems in Atmospheric Chemistry*, edited by J. R. Barker (Singapore: World Scientific).
[10] Molina, M. J., Tso, T. L., Molina, L. T., and Wang, F. C., 1987, *Science*, **238**, 1253.
[11] Tolbert, M. A., Rossi, M. J., Malhotra, R., and Golden, D. M., 1987, *Science,* **238**, 1258.
[12] Leu, M. T., 1988, *Geophys. Res. Lett.*, **15**, 17.
[13] Leu, M. T., 1988, *Geophys. Res. Lett.*, **15**, 851.
[14] Hanson, D. R., and Ravishankara, A. R., 1991, *J. geophys. Res.*, **98**, 5081.
[15] Molina, L. T., and Molina, M. J., 1987, *J. phys. Chem.*, **82**, 2410.
[16] Crutzen, P. J., and Arnold, F., 1986, *Nature*, **324**, 651.
[17] Toon, O. B., Hamill, P., Turco, R. P., and Pinto, J., 1986, *Geophys. Res. Lett.*, **13**, 1284.
[18] Toon, O. B., Turco, R. P., Jordan, J., Goodman, J., and Ferry, G., 1989, *J. geophys. Res.*, **94**, 11359.
[19] Carslaw, K. S., Luo, B. P., Clegg, S. L., Peter, Th., Brimblecombe, P., and Crutzen, P. J., 1994, *Geophys. Res. Lett.*, **21**, 2479.
[20] Tabazadeh, A., Turco, R. P., and Jacobson, M. Z., 1994, *J. geophys. Res.*, **99**, 12897.
[21] Moore, S. B., Keyser, L. F., Leu, M. T., Turco, R. P., and Smith, R. H., 1990, *Nature*, **345**, 333.
[22] Leu, M. T., Moore, S. B., and Keyser, L. F., 1991, *J. phys. Chem.*, **95**, 7763.
[23] Chu, L. T., Leu, M. T., and Keyser, L. F., 1993, *J. phys. Chem.*, **97**, 7779.

[24] Chu, L. T., Leu, M. T., and Keyser, L. F., 1993, *J. phys. Chem.*, **97**, 12798.
[25] Zhang, R., Leu, M. T., and Keyser, L. F., 1994, *J. Phys. Chem.*, **98**, 13563.
[26] Zhang, R., Leu, M. T., and Keyser, L. F., 1995, *Geophys. Res. Lett.*, **22**, 1493.
[27] Zhang, R., Leu, M. T., and Keyser, L. F., 1996, *J. phys. Chem.*, **100**, 339.
[28] Zhang, R., Leu, M. T., and Keyser, L. F., 1997, *J. phys. Chem.* A, **101**, 3324.
[29] Zhang, R., and Leu, M. T., 1997, *J. geophys. Res.*, **102**, 8837.
[30] Kane, S. M., Timonen, R. S., and Leu, M. T., 1999, *J. phys. Chem.* A, **103**, 9259.
[31] Kane, S. M., and Leu, M. T., 2001, *J. phys. Chem.* A, **105**, 1411.
[32] Timonen, R. S., and Leu, M. T., 2002, unpublished results.
[33] Kane, S. M., Caloz, F., and Leu, M. T., 2001, *J. phys. Chem.* A, **105**, 6465.
[34] Danckwerts, P. V., 1970, *Gas-Liquid Reactions* (New York: McGraw-Hill).
[35] Liler, M., 1971, *Reaction Mechanism in Sulphuric Acid* (London: Academic).
[36] Brown, R. L., 1978, *J. Res. Natl. Bur. Stand.*, **83**, 1.
[37] Klassen, J. K., Hu, Z., and Williams, L. R., 1998, *J. geophys. Res.*, **103**, 16197.
[38] Wilke, C. R., and Chang, P., 1955, *AICHE J.*, **1**, 264.
[39] Reid, R.C., Prausnitz, J. M., and Poling, B .E., 1987, *The Properties of Gases and Liquids* (New York: McGraw-Hill).
[40] Houghton, G., 1964, *J. chem. Phys.*, **40**, 1628.
[41] *Handbook of Chemistry and Physics*, 65th Edn, 1984, (Boca Raton, FL: CRC Press).
[42] Gable, C.M., Betz, H. F., and Maron, S. H., 1950, *J. Am. Chem. Soc.*, **72**, 1445.
[43] Zhang, R., Leu, M. T., and Keyser, L. F., 1995, *J. geophys. Res.*, **100**, 18845.
[44] Zhang, R., Wooldridge, P. J., Abbatt, J. P. D., and Molina, M. J., 1993, *J. phys. Chem.*, **97**, 7351.
[45] Robinson, G. N., Worsnop, D. R., Jayne, J. T., Kolb, C. E., and Davidovits, P., 1997, *J. geophys. Res.*, **102**, 3583.
[46] Deno, N. C., and Wisotsky, M. J., 1963, *J. Am. Chem. Soc.*, **85**, 1735.
[47] Leu, M. T., Timonen, R. S., Keyser, L. F., and Yung, Y. L., 1995, *J. phys. Chem.*, **99**, 13203.
[48] Fuchs, N. A., and Sutugin, A. G., 1970, *Highly Dispersed Aerosols* (Ann Arbor, MI: Ann Arbor Science).
[49] Huey, L. G., Hanson, D. R., and Howard, C. J., 1995, *J. phys. Chem.*, **99**, 5001.
[50] Davidson, J. A., Viggiano, A. A., Howard, C. J., Dotan, I., Fehsenfeld, I. C., Albritton, D. L., and Ferhuson, E. E., 1978, *J. chem. Phys.*, **68**, 2085.
[51] Mozurkewich, M., and Calvert, J. G., 1988, *J. geophys. Res.*, **93**, 15889.
[52] Zhang, R., Wooldridge, P. J., and Molina, M. J., 1993, *J. phys. Chem.*, **97**, 8541.
[53] Fried, A., Henry, B., Calvert, J. G., and Mozurkewich, M., 1994, *J. geophys. Res.*, **99**, 517.
[54] Lovejoy, E. R., and Hanson, D. R., 1995, *J. phys. Chem.*, **99**, 2080.
[55] Hu, J. H., and Abbatt, J. P. D., 1997, *J. phys. Chem.* A, **101**, 871.
[56] Hallquist, M., Stewart, D. J., Baker, J., and Cox, R. A., 2000, *J. phys. Chem.* A, **104**, 3984.
[57] Hanson, D. R., and Ravishankara, A. R., 1991, *J. geophys. Res.*, **96**, 17307.
[58] Zeleznik, F. J., 1991, *J. phys. chem. Ref. Data*, **20**, 1157.
[59] Eigen, M., and Kustin, K., 1962, *J. Am. Chem. Soc.*, **84**, 1355.
[60] Arnold, F., Scheid, J., Stilp, Th., Schlager, H., and Reinhardt, M. E., 1992, *Geophys. Res. Lett.*, **19**, 2421.
[61] Karcher, B., Peter, Th., and Ottmann, R., 1995, *Geophys. Res. Lett.*, **22,** 1501.
[62] Burley, J. D., and Johnston, H. S., 1992, *Geophys. Res. Lett.*, **19**, 1363.
[63] Deschamps, J. M. R., 1957, *Comptes Rendus*, **245**, 1432.
[64] Becker, K. H., Kleffmann, J., Kurtenbach, R., and Wiesen, P., 1996, *J. phys. Chem.*, **100**, 14984.
[65] Fenter, F. F., and Rossi, M. J., 1996, *J. phys. Chem.*, **100**, 13765.
[66] Longfellow, C. A., Imamura, Y., Ravishankara, A. R., and Hanson, D. R., 1998, *J. phys. Chem.* A, **102**, 3323.
[67] Shi, Q., Jayne, J. T., Kolb, C. E., Wornsnop, D. R., and Davidovits, P., 2001, *J. geophys. Res.*, **106**, 24259.
[68] Finlayson-Pitts, B. J., and Pitts, J. N. Jr., 1986, *Atmospheric Chemistry: Fundamental and Experimental Techniques* (New York: John Wiley).

[69] Leu, M. T., and Zhang, R., 1999, *Geophys. Res. Lett*, **26**, 1129.
[70] Singh, H. B., O'Hara, D., Herlth, D., Bradshaw, J. D., Sandholm, S. T., Gregory, G. L., Sachse, G. W., Blake, D. R., Crutzen, P. J., and Kanakidou, M. A., 1992, *J. geophys. Res*., **97**, 16,511.
[71] Kames, J., Schweighoefer, S., and Schurath, U., 1991, *J. Atmos. Chem*., **12**, 169.
[72] Kames, J., and Schurath, U., 1995, *J. atmos. Chem*., **21**, 151.
[73] Singh, H.B., Kanakidou, M., Crutzen, P.J., and Jacob, D. J., 1995, *Nature*, **378**, 50.
[74] Wennberg, P. O., Hanisco, T. F., Jaegle, L., Jacob, D. J., Hintsa, E. J., Lanzendorf, E. J., Anderson, J. G., Gao, R. S., Keim, E. R., Donnelly, S. G., Del Negro, L. A., Fahey, D. W., McKee, S. A., Salawitch, R. J., Webster, C. R., May, R. D., Herman, R. L., Proffitt, M. H., Margitan, J. J., Atlas, E. L., Schauffler, S. M., Flocke, F., McElroy, C. T., Bui, T. P., 1998, *Science*, **279**, 49.
[75] Jaegle, L., Javob, D. J., Brune, W. H., Faloona, I. C., Tan, D., Konda, Y., Sachse, G. W., Anderson, B., Gregory, G. L., Vay, S., Singh, H. B., Blake, D. R., and Shelter, R., 1998, *Geophys. Res. Lett*., **25**, 1709.
[76] McKeen, S. A., Gierczak, T., Burkholder, J. B., Wennberg, P. O., Hanisco, T. F., Keim, E. R., Gao, R. S., Liu, S. C., Ravishankara, A. R., and Faney, D. W., 1997, *Geophys. Res. Lett*., **24**, 3177.
[77] Muller, J.-F., and Brasseur, G., 1999, *J. geophys. Res*., **104**, 1705.
[78] Holzinger, R., Warneke, C., Hansel, A., Jordan, A., Lindinger, W., Scharffe, D. H., Schade, G., and Crutzen, P. J., 1999, *Geophys. Res. Lett*., **26**, 1161.
[79] Arnold, F., Burger, V., Droste-Fanke, B., Grimm, F., Krieger, A., Schneider, J., and Stip, T., 1997, *Geophys. Res. Lett*., **24**, 3017.
[80] Snider, J. R., and Dawson, G. A., 1985, *J. geophys. Res*., **90**, 3797.
[81] Zhou, X., and Mopper, K., 1990, *Environ. Sci. Technol*., **24**, 1864.
[82] Betterton, E. A., 1991, *Atmos. Environ* A, **25**, 1473.
[83] Duan, S. X., Jayne, J. T., Davidovits, P., Worsnop, D. R., Zahnister, M. S., and Kolb, C. E. J., 1993, *J. phys. Chem*., **97**, 2284.
[84] Benkelberg, H.J., Hamm, S., and Warneck, P. J., 1995, *Atmos. Chem*., **20**, 17.
[85] Chatfield, R. B., Gardner, E. P., and Calvert, J. G., 1987, *J. geophys. Res*., **92**, 4208.
[86] Huthwelker, T., Peter, Th., Luo, B. P., Clegg, S. L., Carslaw, K. S., and Brimblecombe, P. J., 1995, *J. atmos. Chem*., **21**, 81.
[87] Klassen, J. K., Lynton, J., Golden, D. M., and Williams, L. R., 1999, *J. geophys. Res*., **104**, 26355.
[88] Imamura, T., and Akiyoshi, H., 2000, *Geophys. Res. Lett*., **27**, 1419.
[89] Nagakura, S., Minegishi, A., and Stanfield, K., 1957, *J. Am. Chem. Soc*., **79**, 1033.
[90] Leisten, J. A., and Wright, K. L., 1964, *Proc. Chem. Soc*., 3173.
[91] Duncan, J. L., Schindler, L. R., and Roberts, J. T., 1998, *Geophys. Res. Lett*., **25**, 631.
[92] Murphy, D. M., Thomson, D. S., and Mahoney, M. J., 1998, *Science*, **282**, 1664.
[93] Dentener, F. J., and Crutzen, P. J., 1993, *J. geophys. Res*., **98**, 7149.
[94] Tang, I. N., and Munkelwitz, H. R., 1994, *J. Geophys. Res*., **99**, 18801.
[95] Xu, J., Imre, D., McGraw, R., and Tang, I., 1998, *J. phys. Chem*. B, **102**, 7462.
[96] Imre, D., Xu, J., Tang, I., and McGraw, R., 1997, *J. phys. Chem*. A, **101**, 4191.